Louisiana State University
LSU Digital Commons

LSU Master's Theses | Graduate School

2010

Modeling PM Rotary-Linear Motors with Twin-Stator Using 3D FEMM

Oleksandr Dobzhanskyi
Louisiana State University and Agricultural and Mechanical College

Follow this and additional works at: https://digitalcommons.lsu.edu/gradschool_theses

 Part of the Electrical and Computer Engineering Commons

Recommended Citation

Dobzhanskyi, Oleksandr, "Modeling PM Rotary-Linear Motors with Twin-Stator Using 3D FEMM" (2010). *LSU Master's Theses*. 2519.
https://digitalcommons.lsu.edu/gradschool_theses/2519

This Thesis is brought to you for free and open access by the Graduate School at LSU Digital Commons. It has been accepted for inclusion in LSU Master's Theses by an authorized graduate school editor of LSU Digital Commons. For more information, please contact gradetd@lsu.edu.

MODELING PM ROTARY-LINEAR MOTORS WITH TWIN-STATOR USING 3D FEMM

A Thesis
Submitted to the Graduate Faculty of the
Louisiana State University and
Agricultural and Mechanical College
in partial fulfillment of the
requirements for the degree of
Master of Science in Electrical Engineering
in
The Department of Electrical & Computer Engineering

by
Oleksandr Dobzhanskyi
Bachelor of Industrial Engineering, Kiev National University of Construction and Architecture, 2006; Master of Industrial Engineering, Kiev National University of Construction and Architecture, 2007
December, 2010

ACKNOWLEGEMENTS

I would like to thank my advisor prof. E. Mendrela for guiding me through my work so that my thesis would be a contribution to Electrical Engineering as a science. His encouragement and ability to motivate inspired me for becoming a professional in Power area.

I am very grateful to prof. J. Aravena, for his constant interest to my research. This thesis is dedicated to him. His death is a big loss for me.

I am thankful to prof. S. Mehraeen, and R. Vaidyanathan for their corrections and suggestions.

TABLE OF CONTENTS

LIST OF TABLES

LIST OF FIGURES

ABSTRACT

A rapid growth of automatization nowadays requires electric machines to be adjusted to any technological process. Therefore, a need in machines with two degrees of mechanical freedom (TDMF), which can operate rotationally and linearly, is relatively large. This thesis is directed on the design and study of performance of PM (permanent magnet) rotary-linear synchronous motors with twin-armature as a new type of electric machines which can perform linear, rotational and helical movements. Three stator versions are considered, namely: stator with rotary and linear armatures, two rotary armatures, and two linear armatures. The rotors have PMs skewed with respect to the axial direction. An analysis of motor performance and an influence of PMs skewing on torque and axial force as well as cogging torque are considered. Calculations are based on 2D and 3D FEM (Finite Element Method).

Obtained results show how magnet skewing influences the performance of PM synchronous motors with rotary and linear armatures:

- skewing magnets on the rotor in case of the machine with rotary armature leads to rising of an axial force and decreasing of a rotational one.
- skewing magnets on the rotor in case of the machine with linear armature gives rise to a rotational force. However, with increase of the rotational force, the axial force diminishes.

Optimal skew angle can be reached when the motors can operate rotationally and linearly at the same time.

Cogging torque, cogging force, torque and force ripples and their minimization are also discussed.

CHAPTER 1: INTRODUCTION

1.1 Overview of the Thesis

The motors with two degrees of mechanical freedom (TDMF) were an object of study of many papers in the past [1, 2, 19-21]. Almost all of them concerned induction machines and reluctance motors.

This thesis is focused on 3-phase twin-armature rotary-linear PM (TARLPM) brushless motors.

The following TARLPM brushless motors with three stator versions are considered:

- stator with rotary and linear armatures;
- stator with two rotary armatures;
- stator with two linear armatures.

- **Motor with rotary and linear armatures**

The motor with rotary and linear armatures is a combination of two motors rotary and linear coupled together (Fig. 1.1).

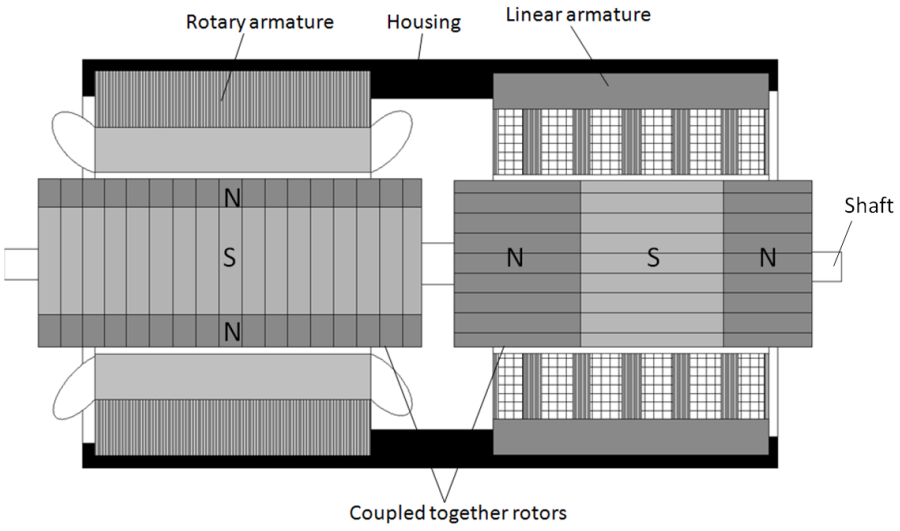

Fig. 1.1 The rotary-linear motor with rotary and linear armatures

The rotary armature generates a rotating magnetic field which interacting with PMs produces a torque, while the magnetic travelling field generated by the linear armature contributes to the axial force. Controlling the input parameters such as voltage and frequency a resultant force and direction of the rotor motion can be changed.

- **Motor with two rotary armatures**

The motor shown schematically in Fig. 1.2 consists of two armatures and associated with them two permanent magnet rotors coupled stiffly together.

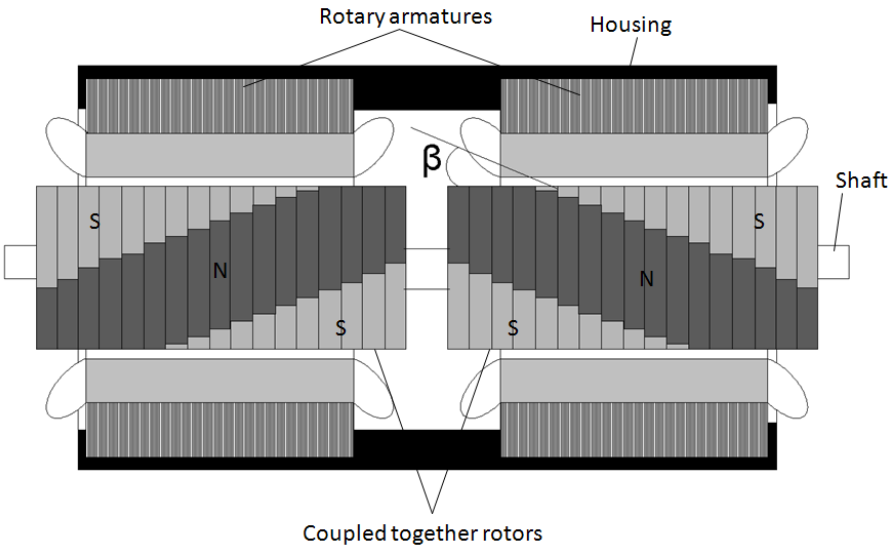

Fig. 1.2 The rotary-linear motor with two rotary armatures

Each armature is built similarly to a conventional AC stator. A 3-phase winding generates a rotating magnetic field. Each rotor has permanent magnets mounted on the ferromagnetic cylinder. The magnets on each of the rotor's parts are skewed with respect to a longitudinal axis in opposite direction by an angle β.

The rotating magnetic flux generated by each armature interacting with permanent magnets gives raise to the force acting on each part of the rotor in the direction perpendicular to the magnet line (Fig. 1.3). Each of the forces F can be split into two components: rotary F_t, and

linear F_z. If the stator magnetic fields rotate with the speed ω_s in the same direction the resultant force that exerts on the rotor is a rotating one (Fig. 1.3a), because two linear components F_z cancel each other. When the magnetic fields rotate in opposite direction the resultant force acts in axial direction only (Fig. 1.3b). By changing a supply voltage in each armature winding the resultant force can be controlled with respect to its direction and magnitude.

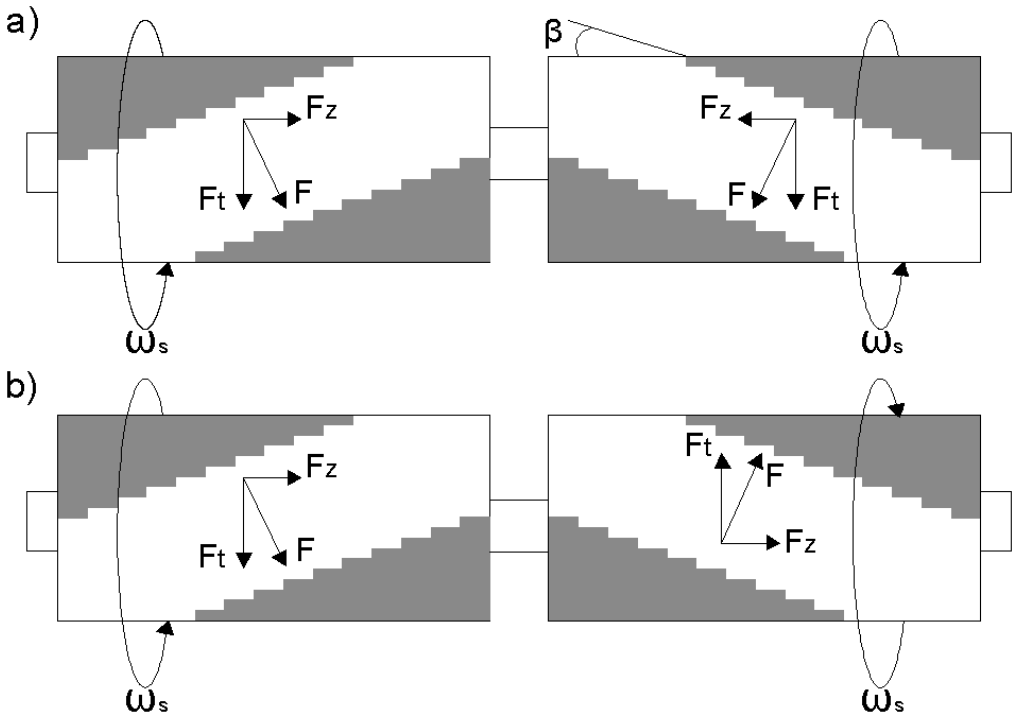

Fig. 1.3 Forces acting on the rotor: F_z - linear force, F_t- rotary force, F – resultant force, ω_s - speed of the rotating magnetic field

- **<u>Motor with two linear armatures</u>**

The motor which is shown schematically in Fig. 1.4 consists of two armatures built similarly to a stator of tubular linear motor, and two associated with them rotors with PMs. Each of the armatures with 3-phase winding generates a linear (traveling) magnetic field moving with speed v_s. Two rotors with surface mounted PMs are coupled together. Permanent magnets on each of

the rotor surfaces are skewed with respect to a longitudinal axis in opposite direction by an angle β.

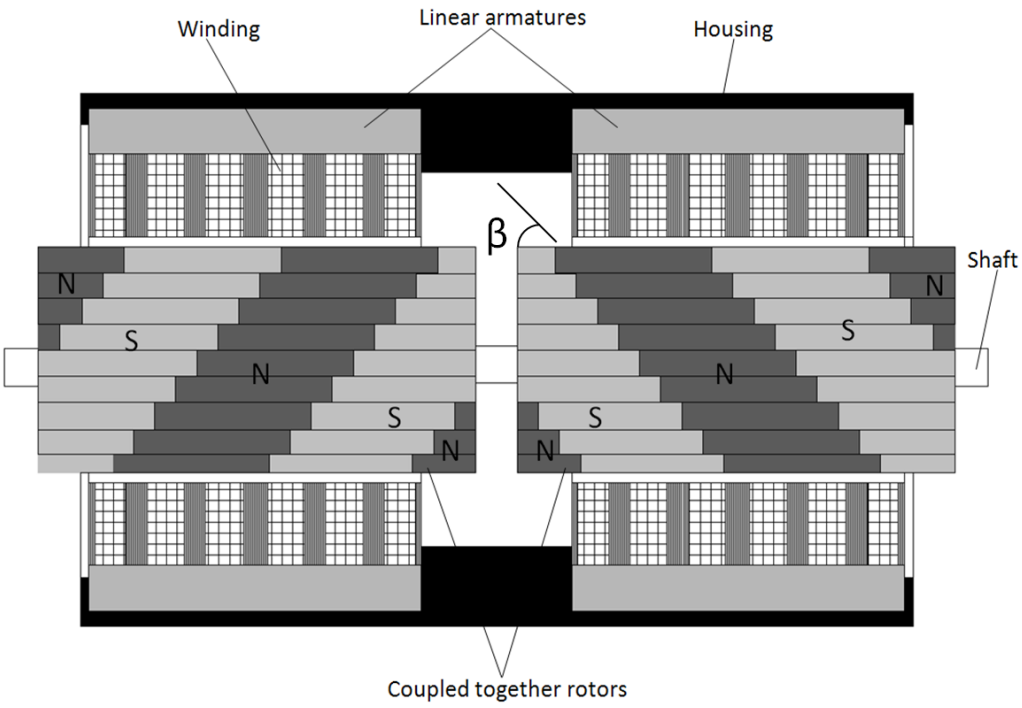

Fig. 1.4 The rotary-linear motor with two linear armatures

Like in case of the motor with rotary armatures, force F which acts on each rotor in the direction perpendicular to magnets line can be split into two components: rotary F_t, and linear F_z.

If the magnetic fields of both armatures travel in opposite direction (Fig. 1.5a) the axial force component F_z cancel each other. Thus, the resultant force acting on the rotor is a rotating one. If the magnetic fields move in the same direction (Fig.1.4.b) the rotary force components F_t cancel each other and the resultant force is equal to the sum of two axial force components F_z.

Changing a direction of traveling magnetic field and the magnitude of the current in each armature, the direction and magnitude of the resultant force can be controlled.

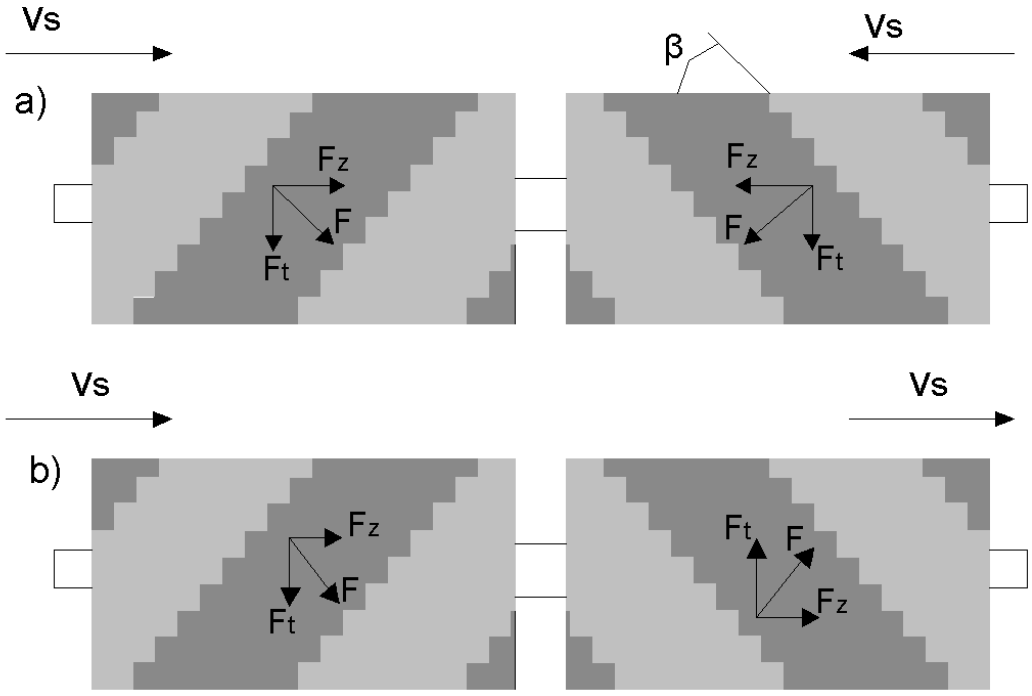

Fig. 1.5 Forces acting on the rotor

The similar idea to that discussed in this thesis is introduced in the paper [21]. In this paper, a new type of rotary-linear permanent magnet motor with two degrees of freedom is designed (Fig.1.6.). Its main performance advantage is its characteristics of decoupling linear and rotary motions.

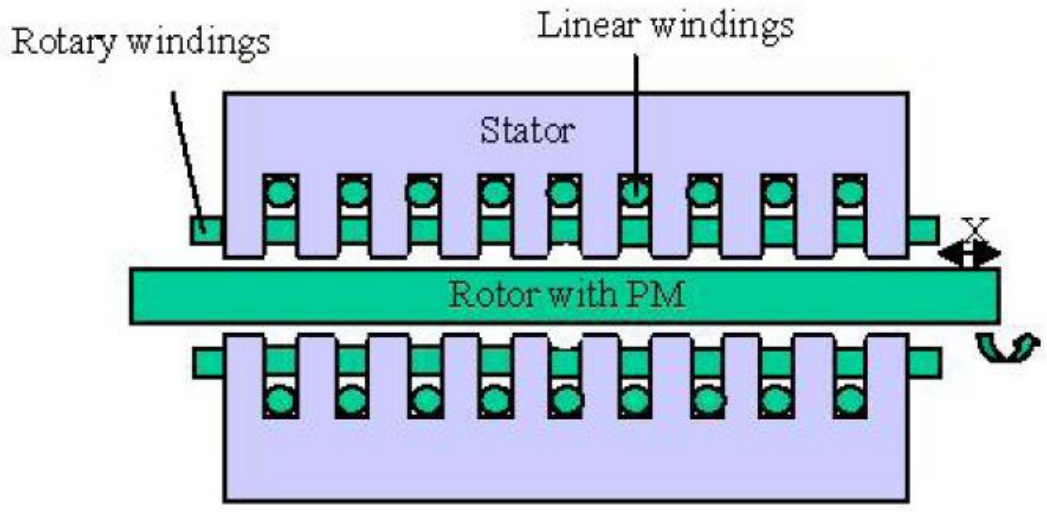

Fig. 1.6 Rotary-linear motor with one armature [21]

The proposed motor consists of two stator three-phase winding systems separately distributed along radial and axial axes. By using independently energized three-phase windings, two space rotating magnetic fields along axial axis and radial axis are achieved, which are utilized to product rotary and linear motion. One special rotor permanent magnet structure capable of generating one radial and one axial magnetic field has been put forward and analyzed to produce enough torque, drag force and decouple rotary and linear motions.

Based on the theoretical analysis and calculation, an experimental motor has been designed and its design process has been detailed introduced in the paper. The validity of analysis and design technique has been confirmed by one three-dimension finite element method (FEM) calculation [21].

As it can been seen from the description of the rotary-linear motor represented in the paper [21] it is quite different from the rotary-linear motors introduced in this thesis. Rotary-linear motors studied in this thesis consist of two armatures, and the motor in the paper [21] is a motor with one armature with two windings (rotary and linear) are placed in one stator.

This thesis is aimed to show how the helical movement of the rotor can be achieved when the motor consists either of rotary and linear armatures, two rotary armatures, and two linear armatures. Also, one of the tasks of the thesis is to study how magnet skew angle affects the forces acting on the rotor. Such a study has not been met in publications, neither the publications on the subject of tubular linear motors which can perform helical movement.

1.2 Objectives of the Thesis

1 To determine the torque and axial force of three types of twin-armature PM rotary-linear motors: with rotary and linear armatures, two rotary armatures, and two linear armatures at the optimum skew angle of rotor PMs.

To find the optimum value of the rotor PM skew angle in three types of rotary-linear motors in order to get the maximum torque and maximum axial force.

2 To optimize the motors' design in order to reduce the torque and force ripples.

1.3 Outline of the Thesis

Chapter 2 discusses PM Synchronous motors. Some basic advantages of PM Synchronous motors over other types of electric machines are outlined.

Chapter 3 provides information about FEM software used in the thesis. Basic Maxwell's equations and approach to solve them using FEM are described. FEM tools used in the thesis such as: FEMM, RM Expert, and Maxwell are presented.

Chapter 4 presents a construction and finite element simulation procedure of a PM synchronous motor with rotary and linear armatures, two rotary armatures, and two linear armatures. Electro-mechanical parameters (torque, axial force, torque and force ripples) are determined. Methods of minimizing of torque and force ripples are introduced. Torque and axial force variation under magnet skewing is studied.

Chapter 5 summarizes the thesis with conclusions made on 3 types of TARLPM motors, and provides a short description of a new type of concrete mixer developed by the author, where TARLPM motors may be used.

CHAPTER 2: PM AC MOTORS

In general, permanent magnet motors are classified into two groups:

- DC PM commutator motors
- AC PM motors

The last group encloses the motors which operate as:

- PM synchronous motors
- Brushless DC motors

Most of the AC PM motors are 3-phase machines. When supplied from AC source of constant frequency (Fig. 2.1) their performance are similar to AC synchronous machines and their speed depends directly on a supply frequency. When the same motor operates with the rotor position feedback loop (see Fig. 2.2) its performance differs significantly from the performance of DC synchronous motors. It behaves like DC motors and its speed depends on a supply voltage and load torque. These types of motors are called brushless DC motors.

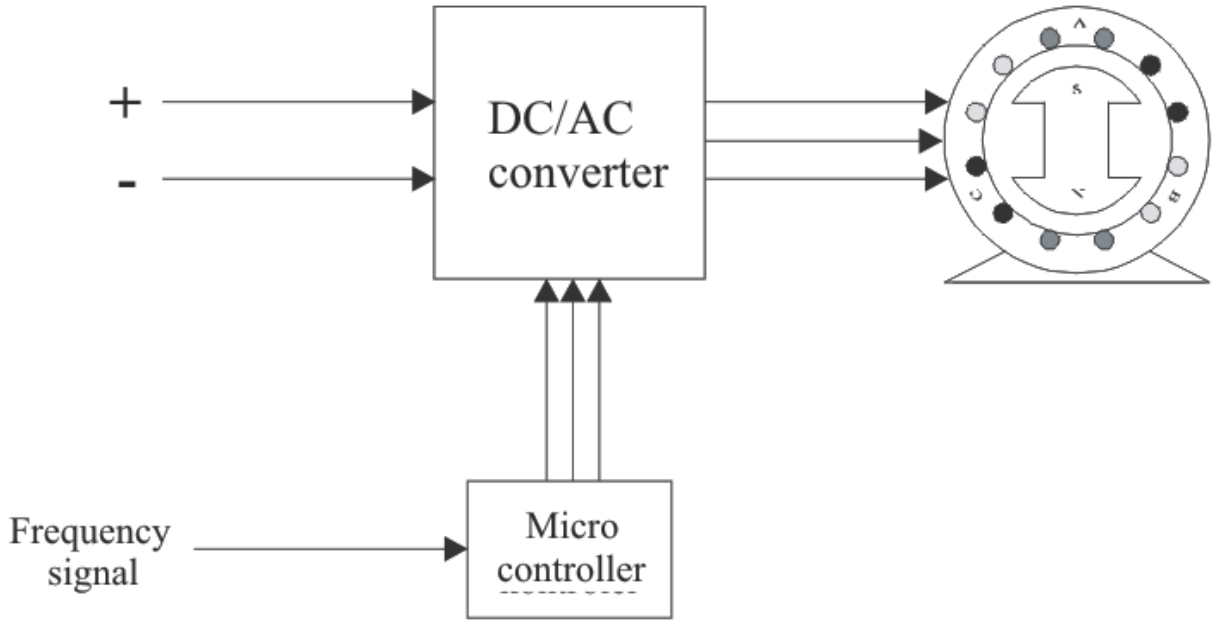

Fig. 2.1 Supply circuit for a brushless PM synchronous motor [22]

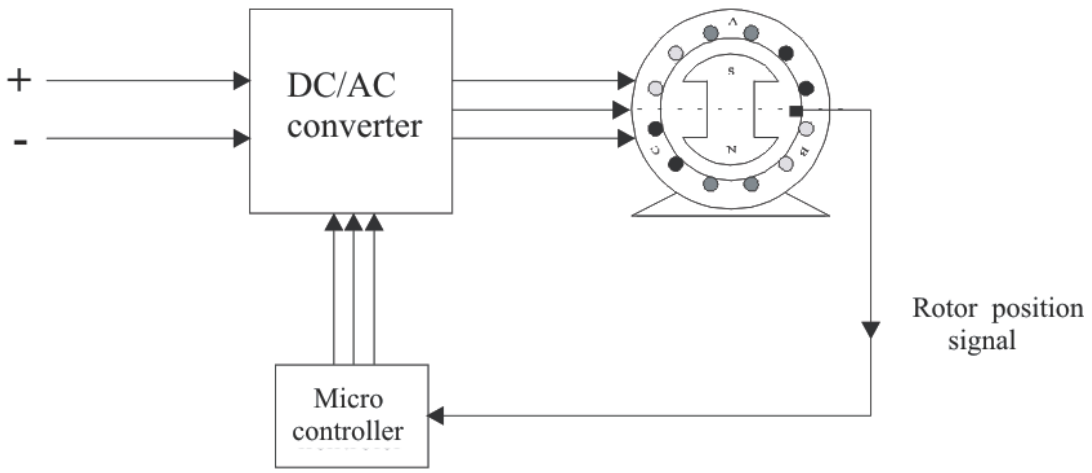

Fig. 2.2 Supply circuit for a brushless PM DC motor [22]

New types of Two-Degree of Mechanical Freedom (TDMF) motors which are proposed in the thesis are PM 3-phase motors which can operate as brushless synchronous motors or brushless DC motors. Such motors have several advantages over other types of PM motors. The armature current of brushless AC motors is not transmitted through brushes, which are subject to wear and require maintenance. Another advantage of the PM AC motors is the fact that the power losses occur in the stator, where heat transfer conditions are good. Consequently, the power density can be increased as compared with a DC commutator motor. In addition, considerable improvements in dynamics can be achieved because the air-gap magnetic flux density is high, the rotor has a lower inertia and there are no speed-dependent current limitations. Thus, the volume of a brushless PM motor can be reduced by more than 40% while still keeping the same rating as that of a PM commutator DC motor.

PM AC motors are used in a broad power range from mWs to hundreds kWs. Thus, PM motors cover a wide variety of application fields, from stepping motors for wrist watches, through industrial drives for machine tools to large PM synchronous motors for ship propulsion (navy frigates, cruise ships, medium size cargo vessels and ice breakers) [3].

DESCRIPTION OF 2D AND 3D FINITE ELEMENT METHOD (FEM) SOFTWARES USED IN THE THESIS

3.1 Finite Element Method

The Finite Element Method (FEM) has been developed into a key, indispensable technology in the modeling and simulation of advanced engineering systems in various fields like housing, transportation, communications, and so on. The FEM was first used to solve problems of stress analysis, and has since been applied to many other problems like thermal analysis, fluid flow analysis, piezoelectric analysis, and others. Basically, the analyst seeks to determine the distribution of some field variable like the displacement in stress analysis, the temperature or heat flux in thermal analysis, the electrical charge in electrical analysis, and so on. The FEM is a numerical method seeking an approximated solution of the distribution of field variables in the problem domain into several elements.

In this thesis FEM is used to solve magnetostatic problems. Because of that some basic electromagnetic equations will be reviewed first.

Magnetostatic problems are problems in which the magnetic field is time-invariant. In this case, the field intensity (*H*) and flux density (*B*) must obey:

$$\nabla \cdot H = J \tag{3.1}$$

$$\nabla \cdot B = 0 \tag{3.2}$$

where J is a current density.

Constitutive relationship between *B* and *H* for each material:

$$B = \mu \cdot H \tag{3.3}$$

If a material is nonlinear, the permeability μ is a function of *B*:

$$\mu = \frac{B}{H(B)} \tag{3.4}$$

FEM is used to find a field that satisfies Eqns. (3.1 – 3.3) via a magnetic vector potential approach. Flux density is written in terms of the vector potential *A*, as:

$$B = \nabla \cdot A \tag{3.5}$$

This definition of *B* always satisfies Eqn. (3.2). When substituted into Eqns. (3.1) can be rewritten as:

$$\nabla \cdot \frac{1}{\mu_B} \nabla \cdot A = J \tag{3.6}$$

For a linear isotropic material, Eqn. (3.6) reduces to:

$$-\frac{1}{\mu} \nabla^2 \cdot A = J \tag{3.7}$$

FEM retains the form of (3.6), so that magnetostatic problems with a nonlinear *B*-*H* relationship can be solved.

In the general 3-D case, *A* is a vector with three components. However, in the 2-D planar and aximmetric cases, two of these three components are zero, leaving just the component in the "out of the page" direction.

The advantage of using the vector potential formulation is that all the conditions to be satisfied have been combined into a single equation. If *A* is found, *B* and *H* can then be deduced by differentiating *A*. The form of Eqn. (3.6), an elliptic partial differential equation, and it arises in the study of many different types of engineering phenomena.

The behavior of a phenomenon in a system depends upon the geometry or domain of the system, the property of the material or medium, and the boundary, initial and loading conditions.

The procedure of computational modeling using FEM broadly consists of four steps:

- Modeling of the geometry;
- Meshing (discretization);

- Specification of material property;
- Specification of boundary, initial and loading conditions.

- **Modeling of the geometry**

Real structures, components or domains are in general very complex, and have to be reduced to a manageable geometry. Curved parts of the geometry and its boundary can be modeled using curves and curved surfaces. However, it should be noted that the geometry is eventually represented by piecewise straight lines of flat surfaces, if linear elements are used. The accuracy of representation of the curved parts is controlled by the number of elements used. It is obvious that with more elements, the representation of the curved parts by straight edges would be smoother and more accurate. Unfortunately, the more elements, the longer is the computational time that is required. Hence, due to the constraints on computational hardware and software, it is always necessary to limit the number of elements.

- **Meshing**

Meshing is performed to descretize the geometry created into small pieces called elements or cells. The solution for an engineering problem can be very complex and if the problem domain is divided (meshed) into small elements or cells using a set of grids or nodes, the solution within an element can be approximated very easily using simple functions such as polynomials. Thus, the solutions for all of the elements form the solution of the whole problem domain. Mesh generation is a very important task of the pre-process. It can be a very time consuming task to the analyst, and usually an experienced analyst will produce a more credible mesh for a complex problem. The domains have to be meshed properly into elements of specific shapes such as triangles and quadrilaterals. Triangle mesh of the PM synchronous machine is shown in Fig. 3.1

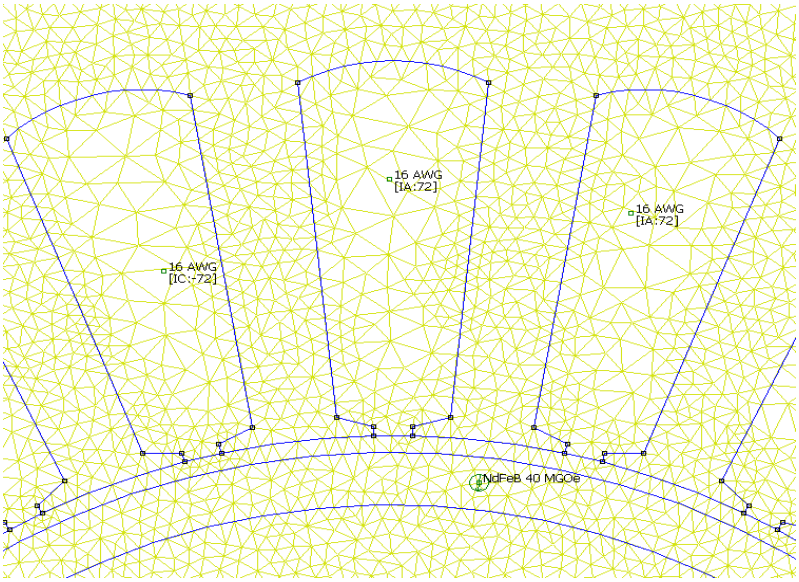

Fig. 3.1 Triangle mesh

- **Property of material or medium**

Many engineering systems consist of more than one material. Property of materials can be defined either for a group of elements or each individual element, if needed. For different phenomena to be simulated, different sets of material properties are required. For, example, Youg's modulus and shear modulus are required for the stress analysis of solids and structures whereas the thermal conductivity coefficient will be required for a thermal analysis. Input of material's properties into a pre-processor is usually straightforward. All the analyst needs to do is select material properties and specify either to which region of the geometry or which elements the data applies.

- **Boundary, initial and loading conditions**

Boundary, initial and loading conditions play a decisive role on solving the simulation. To input these conditions is usually done using commercial pre-processor, and it is often interfaced with graphics. Users can specify these conditions either to the geometrical identities (points, lines or curves, surfaces, and volumes) or to the elements or grid [24].

There are many commercially used FEM programs. Three programs are used in this thesis to model the PM rotary-linear motors. These are: FEMM 4.0 [15], Maxwell 12v [4], and RM Expert [4].

3.2 FEMM 4.0

FEMM 4.0 is a suite of programs for solving low frequency electromagnetic problems of two-dimensional planar and axisymmetric domains. The program currently addresses linear/nonlinear magnetostatic problems, linear/nonlinear time harmonic magnetic problems, linear electrostatic problems, and steady-state heat flow problems.

FEMM is divided into three parts:

• Interactive shell (femm.exe). This program is a Multiple Document Interface pre-processor and a post-processor for the various types of problems solved by FEMM. It contains a CAD like interface for laying out the geometry of the problem to be solved and for defining material properties and boundary conditions. Autocad DXF files can be imported to facilitate the analysis of existing geometries. Field solutions can be displayed in the form of contour and density plots. The program also allows the user to inspect the field at arbitrary points, as well as evaluate a number of different integrals and plot various quantities of interest along user-defined contours.

• triangle.exe. Triangle breaks down the solution region into a large number of triangles, a vital part of the finite element process

• Solvers.

- *fkern.exe* - for magnetics;
- *belasolv* - for electrostatics;
- *hsolv* - for heat flow problems;

- *csolv* - for current flow problems. Each solver takes a set of data files that describe problem and solves the relevant partial differential equations to obtain values for the desired field throughout the solution domain.

The Lua scripting language is integrated into the interactive shell [15].

FEMM 4.0 was used in this thesis mainly to compute the torque and linear force of the motor in order to check the results with those obtained from modeling in 3D FEM software. Lua script was applied to link Matlab and FEMM to calculate torque of PM Motor with rotary armature when magnets were skewed.

3.3 Maxwell 12v

Maxwell 12v is an interactive software package that uses finite element method to solve three-dimensional (3D) electrostatic, magnetostatic, Eddy current and transient problems. It is used to compute:

• Static electric fields, forces, torques, and capacitances caused by voltage distributions and charges.

• Static magnetic fields, forces, torques, and inductances caused by DC currents, static external magnetic fields, and permanent magnets.

• Time-varying magnetic fields, forces, torques, and impedances caused by AC currents and oscillating external magnetic fields.

• Transient magnetic fields caused by electrical sources and permanent magnets [4].

In the thesis magnetostatic and transient solvers were used.

3.4 RM Expert

Rotational Machine Expert (RM Expert) is an interactive software package used for designing and analyzing electrical machines.

Using RM Expert, following types of machines can be simulated:

• Three-phase and single-phase induction motors.

• Three-phase synchronous motors and generators.

• Brushless permanent-magnet DC motors.

• Adjust-speed synchronous motors and generators.

• Permanent-magnet DC motors.

• Switched reluctance motors.

• Line-start permanent-magnet synchronous motors.

• Universal motors.

• General DC motors and generators.

• Claw-pole alternators [4].

RM Expert is 2D software. In the thesis it was applied to calculate cogging torque, and air-gap flux density of the PM motor with rotary armature.

CHAPTER 4: TARLPM MOTORS WITH TWIN ARMATURE

4.1 General Description of TARLPM Motor with Rotary and Linear Armatures

The motor that is considered with its main dimensions is shown schematically in Fig. 4.1

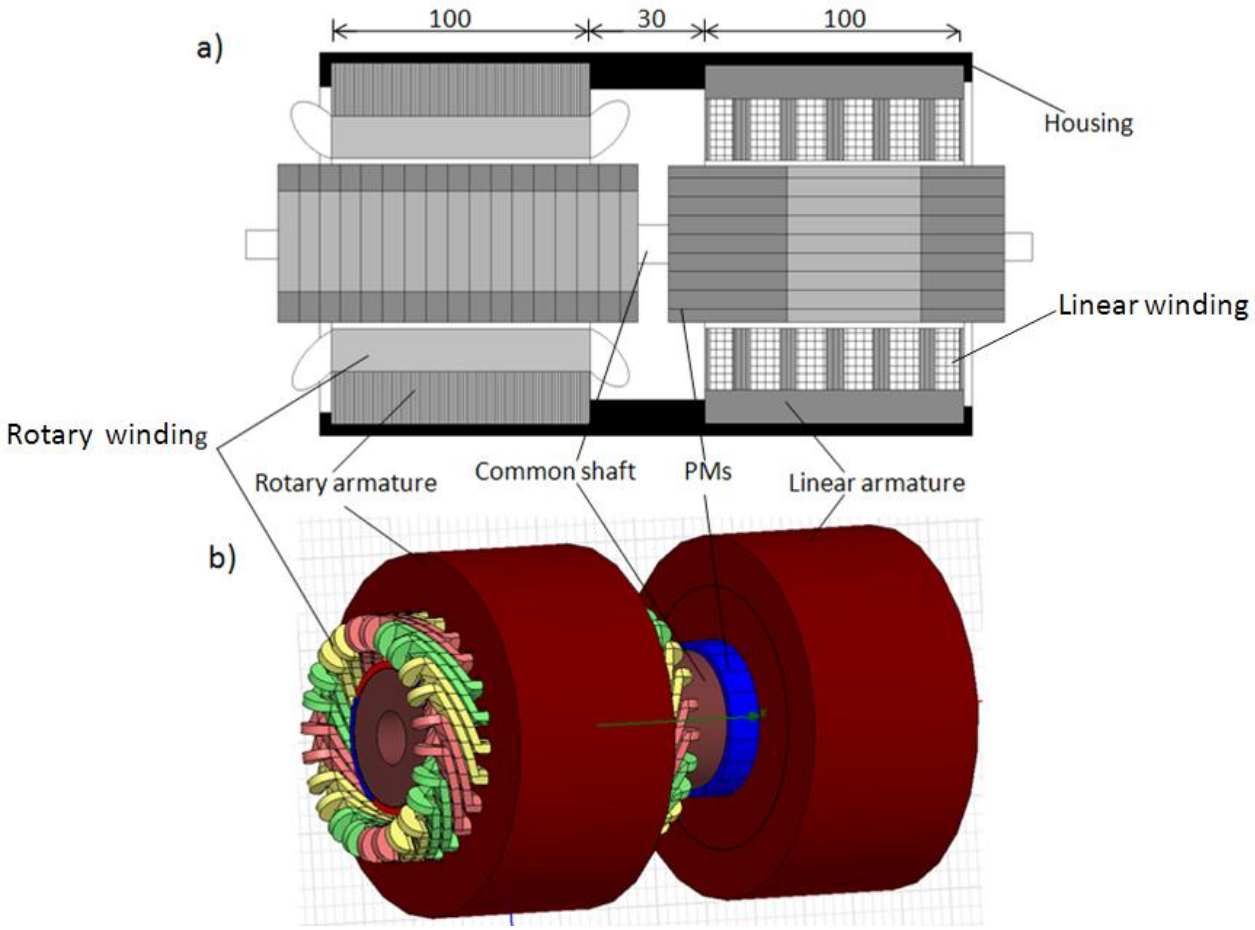

Fig.4.1Motor with rotary and linear armatures

The operation of the motor can be analyzed as the operation of two motors: rotary and linear working independently with the rotors coupled stiffly together. This type of approach can be applied under the condition that there is no any magnetic link between the armatures and the motion of one rotor does not influence the work of another one. This assumption is fulfilled if there is a long enough distance between the armatures and the axial speed of the rotors is low [16].

In case of the analyzed motor here both conditions are satisfied and the analysis of each part of the TARLPM motor can be carried out separately as the analysis of PM 3-phase rotary and linear motors. This is done in the following sections.

In case of high linear speed, linear motion influences the performance of rotary motor. The phenomenon that occurs is a part of *end effects*. The nature of these effects are described and analyzed in the papers [17, 18].

The analysis is concentrated only on a torque and axial force produced by the motor. These are determined for the TARLPM motor of particular dimensions using FEM.

4.2 PM Motor with Rotary Armature

4.2.1 Design Parameters of PM Motor with Rotary Armature

The motor under consideration is shown on Fig. 4.2.

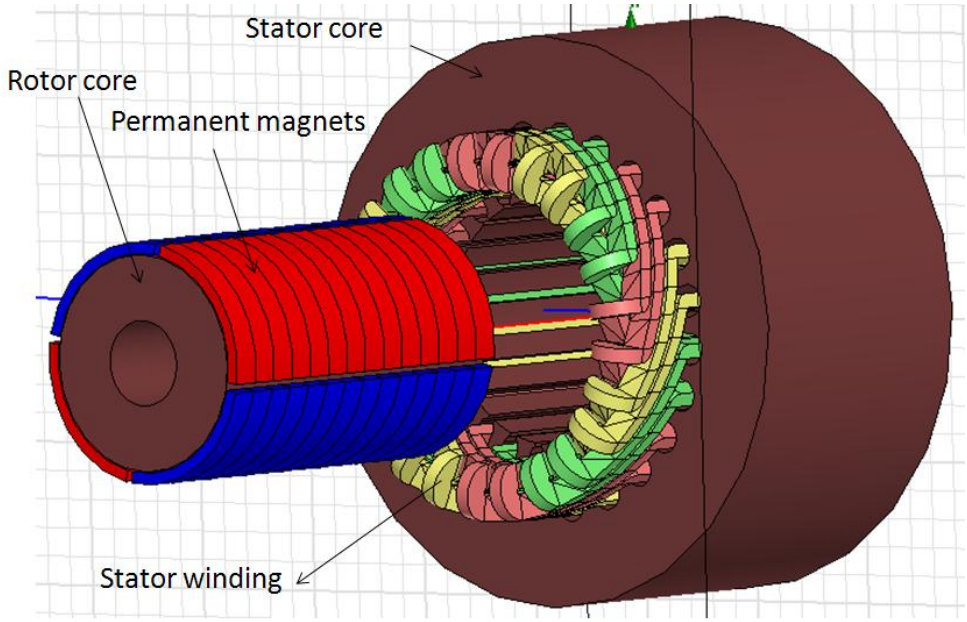

Fig. 4.2 PM 3-phase motor with rotary armature

The motor consists of a stator made of laminated steel (US Steel 1008), winding, solid iron rotor core and permanent magnets glued on its surface. Permanent magnets and winding data are enclosed in Table 4.1. Basic dimensions of the machine are shown in Fig. 4.3.

Winding is distributed in slots according to the winding diagram shown in Fig. 4.4. To determine the torque it was assumed that the winding was supplied with 3-phase sinusoidal rated current rms value of $I_{rat}(rms) = 9.2\ A$.

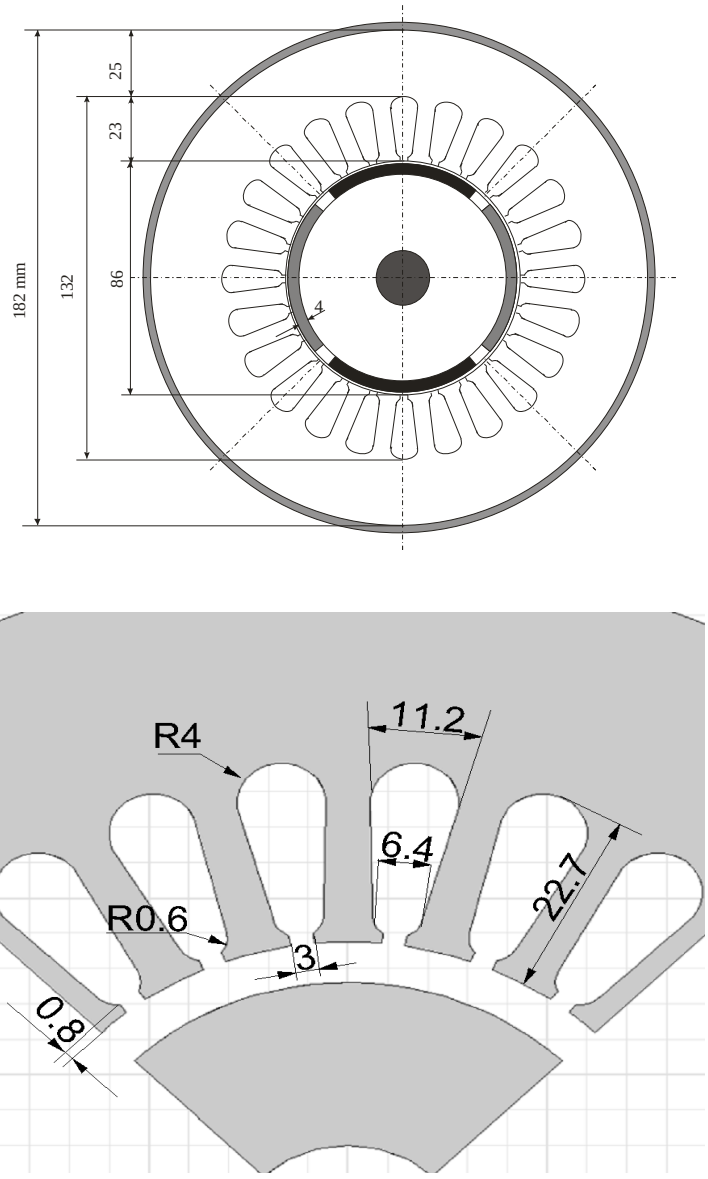

Fig. 4.3 Rotary motor dimensions

Table 4.1 Winding and magnets data for PM motor with rotary armature

Winding:	
- Number of phases	3
- Number of poles	4
- Number of slots per pole per phase	2
- Number of wires per slot, N_w	72
- Filling factor, K_{Cu}	0.5
- Wire	AWG16
Air gap width, mm	1
Permanent magnets (PMs):	
- Type	NdFe40,
- Relative permeability	1.09967
- Bulk conductivity, S/m	625000
- Residual flux density B_r, Tesla	1.24T

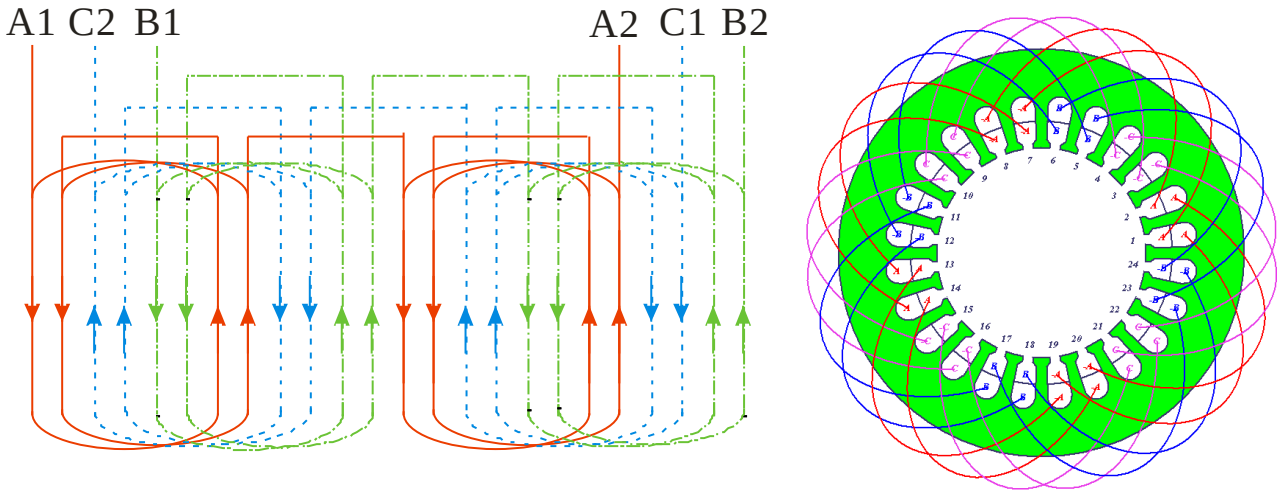

Fig. 4.4 Rotary winding diagram

B-H characteristics for stator core laminated steel and rotor core iron are shown in Fig.4.5 a, b.

a)

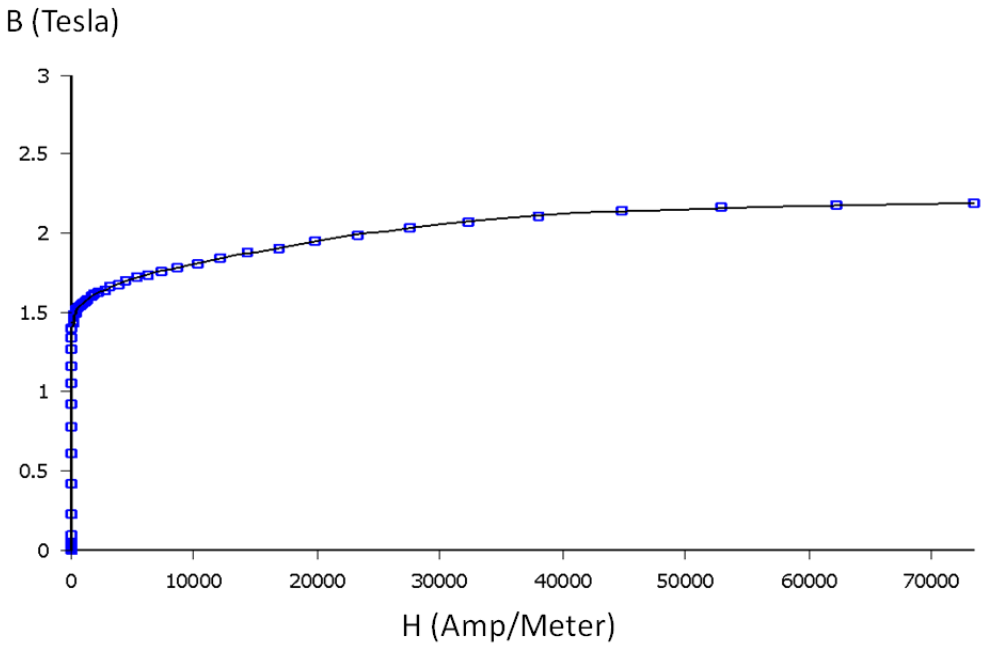

b)

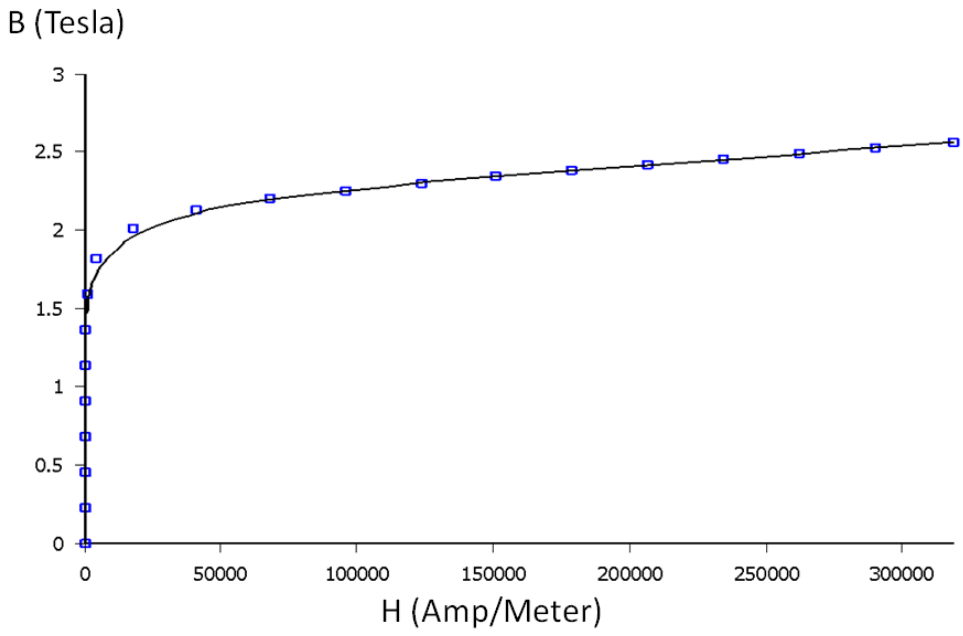

Fig. 4.5 Magnetization characteristic of (a) stator core, (b) rotor core [15]

4.2.2 Magnetic Flux Density

One of the most important quantities in electric machines is magnetic flux density in the air-gap B_{mg}. It decides about the value of electromagnetic torque and motor performance. The magnetic flux density distribution in the air-gap together with current distribution in the winding allows to predict the torque produced by the motor according to the basic equation:

$$T_{em} = k \cdot B_{mg} \cdot J \tag{4.1}$$

where J is the linear current density on the stator surface, and k is a constant.

The knowledge about distribution of the magnetic flux density in the stator and rotor cores gives the information on how the magnetic material is utilized if it is saturated or not.

With respect to the above statement, the calculation of the magnetic flux density was done using the 2D and 3D FEM software.

Fig. 4.6 shows the flux density distribution in the middle of the air-gap. It was determined at stator load current using RM Expert software.

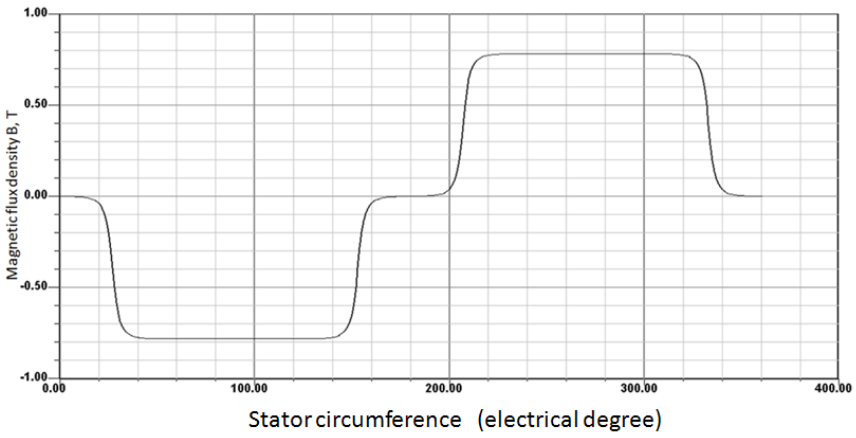

Fig. 4.6 Magnetic field density in the middle of the air gap

Since the rotor has surface mounted permanent magnets of 3.5mm thickness the flux generated by stator current almost does not affect the magnetic field of the permanent magnets and the flux density over the magnet length has constant value (see Fig. 4.6).

Magnetic field density distribution lines obtained from FEMM (a) and Maxwell 3D (b) and is plotted in Fig. 4.7. Fig. 4.7a represents the flux density distribution obtained from FEMM 4.0 and Fig. 4.7b shows magnetic flux density distribution determined in the middle of the motor length by Maxwell.

a)

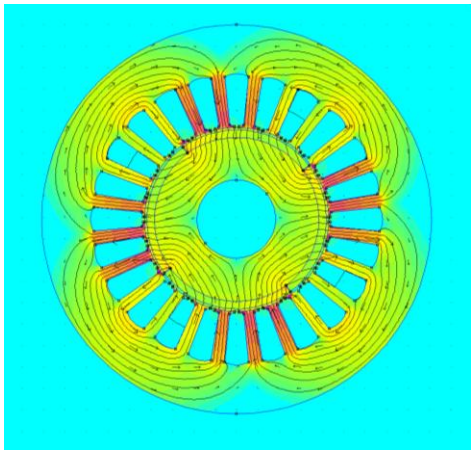

b)

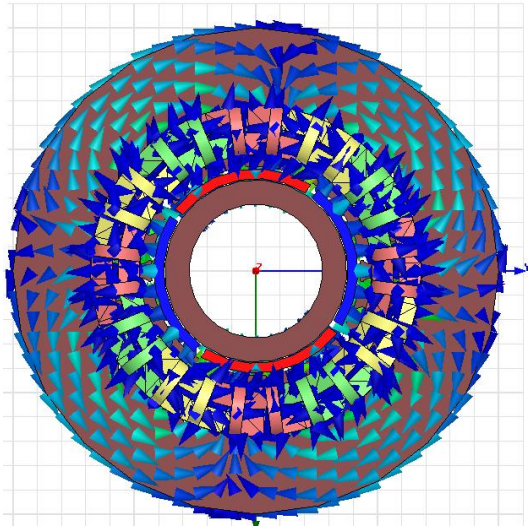

Fig.4.7 Magnetic field density in the stator and rotor from FEMM (a) and Maxwell 12v 3D (b)

The results obtained from FEMM 4.0 and Maxwell do not differ, and the obtained maximum flux density in the motor cores are: for stator – 1.4T, rotor – 1.1T. In further calculations of flux density, Maxwell 12v 3D will be used only.

The accuracy of the finite element solution is dependent on the mesh topology [3]. Fig. 4.8 shows the motor model built in FEMM 4.0 with the relatively high density mesh what enables to obtain high accuracy in the flux calculation.

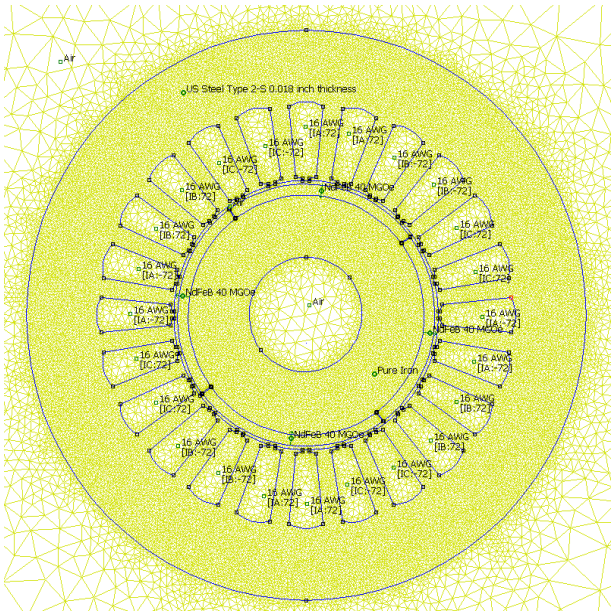

Fig. 4.8 Mesh of the motor obtained using FEMM 4.0

This, however, makes the time period of calculation very long. The number of nodes related to this model is 5298. 3D Maxwell model had the mesh size at which the calculation error is less than 1%.

4.2.3 Electromagnetic Torque

As it was mentioned in Chapter 2 the motor can operate either as synchronous or brushless DC motor. In later case the vector of the rotor magnetic flux Φ_r is always perpendicular to the resultant vector of the stator current $\imath_s$ as shown in Fig. 4.9a [5]

This allows obtaining the maximum electromagnetic torque T_{em} which expressed in terms of angle δ is:

$$T_{em} = T_{max} \cdot sin\delta \tag{4.2}$$

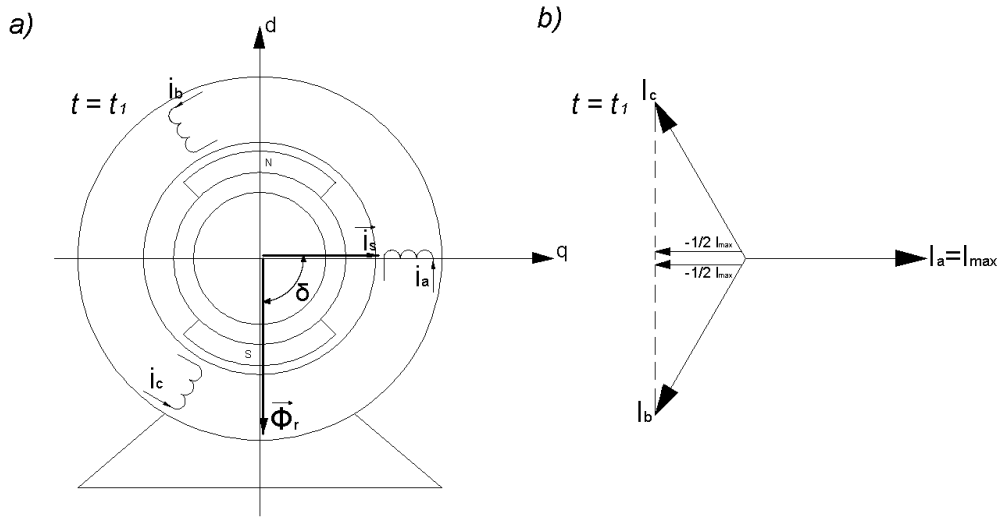

Fig. 4.9 a) Magnetic flux and resultant current vectors in a d-q system, b) Current phasor diagram of time instant t_1

where T_{max} is the torque developed when vectors Φ_r and $\imath_s$ are perpendicular to each other.

Such a configuration of rotor flux and stator current vectors is in DC brushless motors what justifies the name of the analyzed AC motor: "brushless DC motor".

To obtain rotor flux vector perpendicular to current vector the 3-phase currents must be switched in time by 3-phase inverter in the proper sequence, what is possible due to the rotor position sensor (see Fig. 2.2). For the rotor position shown in Fig. 4.10a the currents phasors have to be at this time instant t_1 as in Fig. 4.10b. It means that rms stator current is equal to 9.2 A. The phases in 3 phases have the values: $i_a = 13A,\ i_b = -6.5A\ , i_c = -6.5A$.

a)

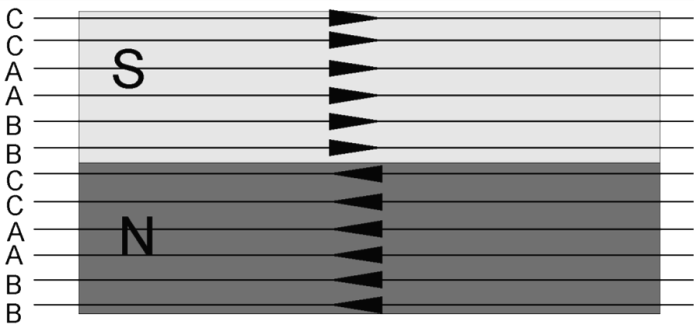

Fig. 4.10 Stator winding actual currents position with respect to the rotor magnets

(Fig. 4.10 cont.)

b)

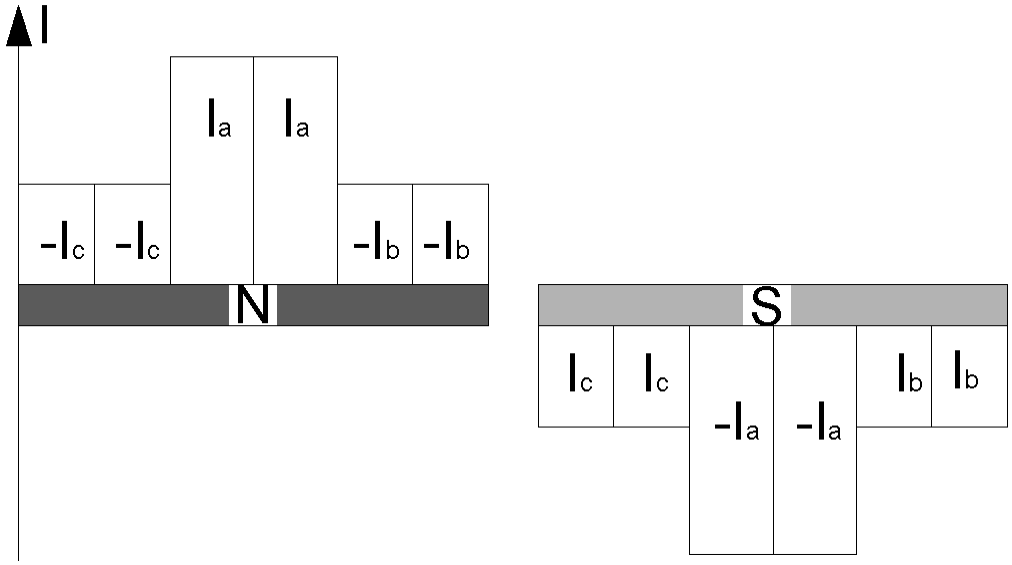

The torque was calculated using 2-D and 3-D programs: FEMM, RM Expert, 3D Maxwell in order to check the differences between them. The results are presented in Table 4.2

Table 4.2 Torque of the motor calculated using different software

Software	FEMM	RM Expert	**3D Maxwell**
Torque (Nm)	54.5	54.9	**55.2**

The discrepancies between results are less than 2%. It means that more simple 2-D FEM program can be used also in the calculations

4.2.4 Cogging Torque

Cogging torque is an inherent characteristic of PM machines with slotted cores and it is caused by the geometry of the motor [6]. Cogging torque in brushless motors comes from variations in magnetic field density around a rotor's permanent magnets as they pass the non-

uniform geometry of the slot openings in the stator [9]. Cogging torque affects self-start stability and produces noise and mechanical vibration. The cogging torque is independent on the stator currents (load). The frequency of the cogging torque is:

$$f = \frac{z_1}{p/2} f \tag{4.3}$$

where z_1 is the number of stator slots, p is the number of poles, and f is the input frequency. Neglecting the energy stored in the ferromagnetic core, the cogging torque is expressed as:

$$T_c = \frac{dW}{d\theta} = \frac{D_{2out}}{2} \frac{dW}{dx} \tag{4.4}$$

where $D_{2out} \approx D_{1in}$ is the rotor outer diameter, $\theta = 2x/D_{2out}$ is the mechanical angle, and W is the magnetic field energy in the air-gap.

It is very important to determine the cogging torque before manufacturing.

Cogging torque versus mechanical angle developed within the range of two teeth of the motor is shown in Fig. 4.11. It was calculated by RM Expert software .

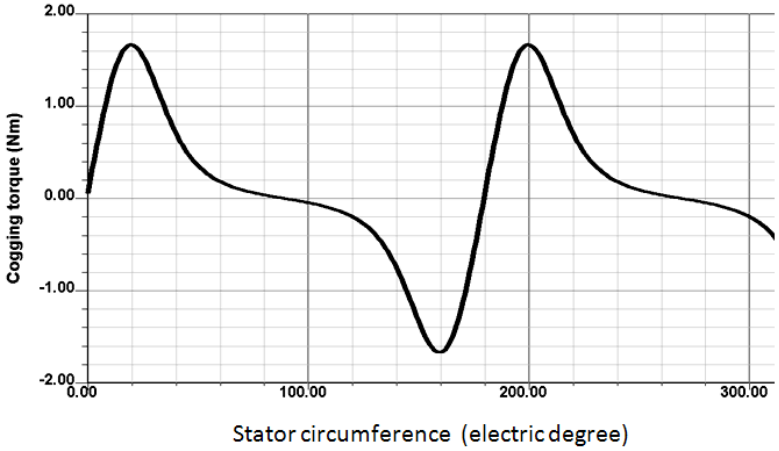

Fig. 4.11 Cogging torque

There are many techniques to minimize cogging torque [5-9]. One of them is skewing stator slots by one tooth-pitch with respect to the axially placed PMs. In case of the presented motor

cogging torque can be minimized if the permanent magnets are skewed with respect to the stator slots by the angle being the multiplication of tooth-pitch (Fig. 4.12).

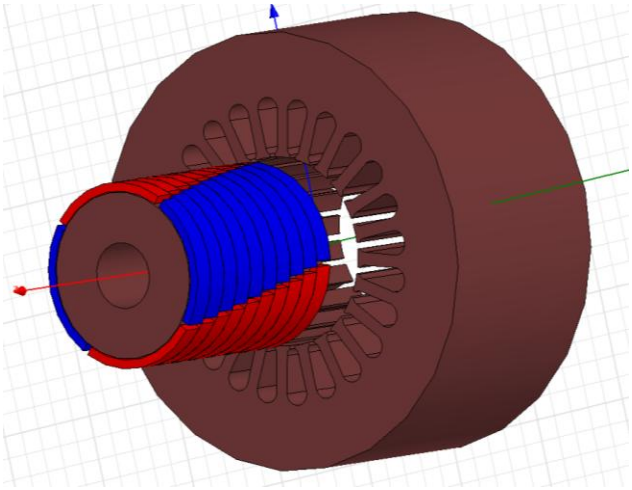

Fig. 4.12 Motor with magnets skewed on the rotor for one tooth-pitch

The cogging torque of the model with skewed magnets shown in Fig. 4.13 is 59% lower than that obtained when magnets were not skewed (see Fig. 4.11).

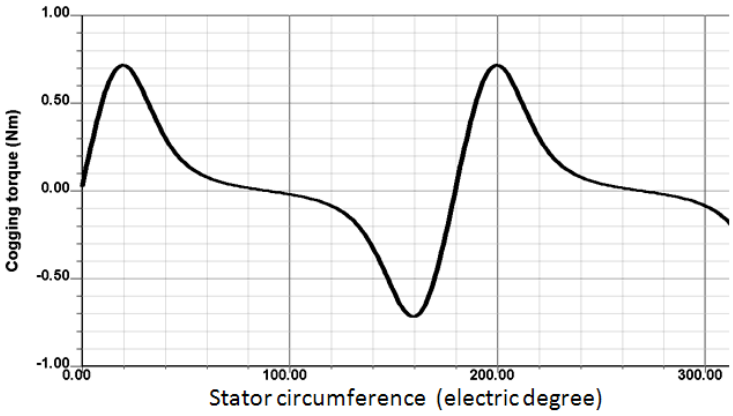

Fig. 4.13 Cogging torque (magnets are skewed)

However, the electromagnetic torque gets down with magnet skewing. The influence of magnet skewing on torque is studied in the section 4.4.

Despite the cogging torque of the motor is reduced due to magnet skewing there is still torque ripple produced by the fact that phase winding are not sinusoidal distributed on the stator circumference. It would be more visible if phase current waveforms had square shape instead of sinusoidal one.

The instantaneous torque of an electrical motor:

$$T\ \alpha\ = T_0 + T_r(\alpha) \tag{4.5}$$

has two components:

- constant or average component T_0;
- periodic component $T_r(\alpha)$, which is a function of time or angle α, superimposed on the constant component.

The periodic component causes the torque pulsations called also torque ripple. Torque ripple can be defined as [3]:

$$t_r = \frac{T_{max} - T_{min}}{T_{max} + T_{min}} \tag{4.6}$$

Torque ripple of the motor is shown in Fig. 4.14. Due to complexity of the model and simulation algorithm, the graph waveform is not smooth because only several steps of calculation were undertaken. The main task was to determine T_{max} and T_{min} which are calculated precisely.

According to the formula (4.11) we have:

$$t_r = \frac{T_{max} - T_{min}}{T_{max} + T_{min}} = \frac{58 - 52}{58 + 52} = 0.054\ or\ 5.4\%$$

There are three sources of torque ripple coming from the machine:

- cogging effect (detent effect), i.e., interaction between the rotor magnetic flux and variable permeance of the air gap due to the stator slot geometry;
- distortion of sinusoidal or trapezoidal distribution of the magnetic flux density in the air gap;
- the difference between permeances of the air gap in the *d* and *q* axis [3].

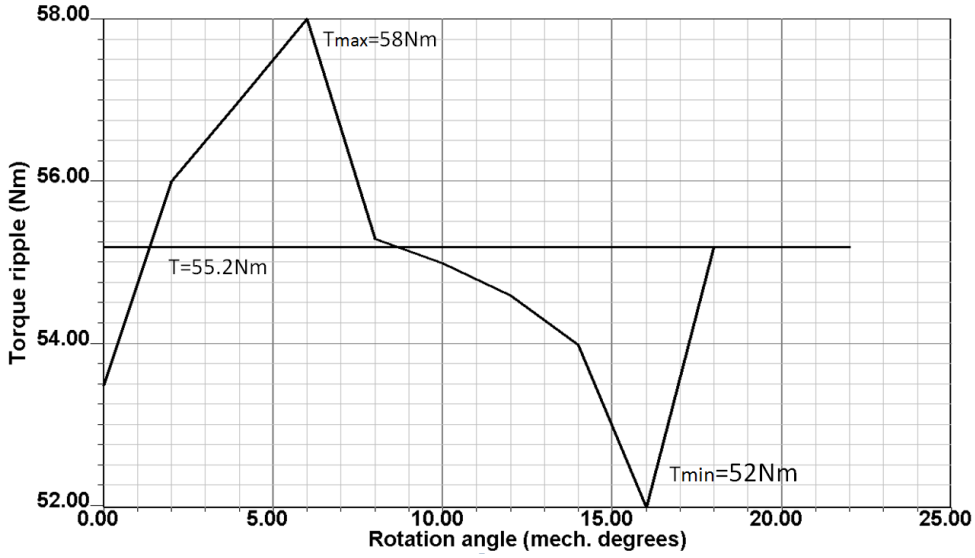

Fig. 4.14 Torque ripple

From these sources we will mainly concentrate on interaction of rotor magnetic flux with stator slot geometry. The minimization of torque ripple in PM motor with two rotary armatures is discussed in the section 4.4.

4.3 PM Motor with Linear Armature

4.3.1 Design Parameters of PM Motor with Linear Armature

The second part of the PMRL motor with rotary and linear armature is shown in Fig. 4.15. It consist of a stator core made of laminated steel, solid iron rotor with permanent magnets glued on its surface, and winding placed in the stator slots. Motor dimensions are shown in Fig. 4.16. Winding and magnets data are enclosed in Table 4.3.

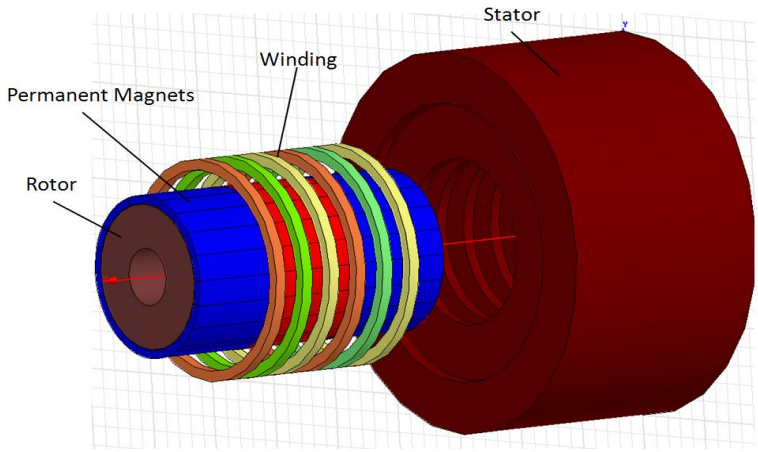

Fig. 4.15 Motor with linear armature

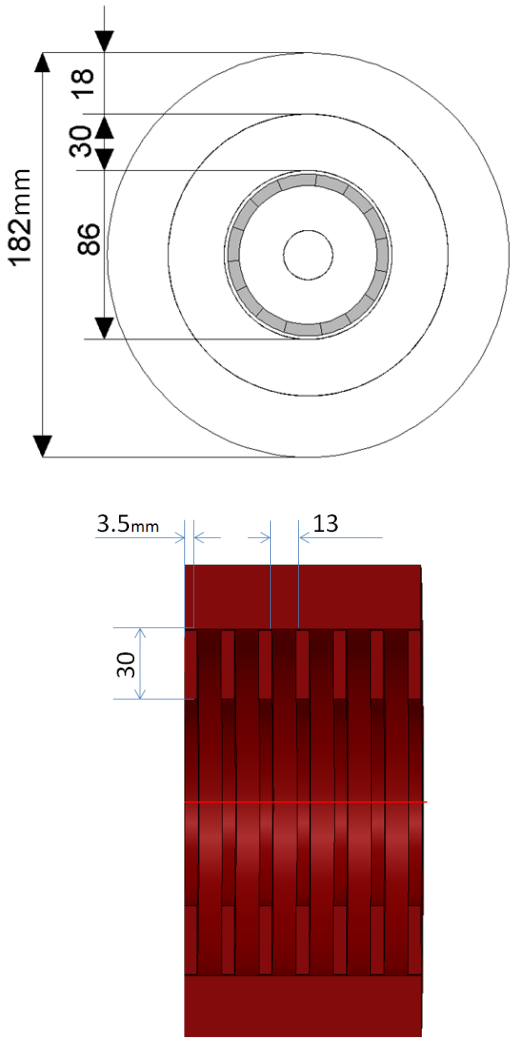

Fig. 4.16 Motor dimensions

Table 4.3 Winding and magnets data for PM motor with linear armature

Winding:	
- Number of phases	3
- Number of poles	2
- Number of slots per pole per phase	1
- Number of wires per slot, N_w	115
- Filling factor, K_{cu}	0.5
- Wire	AWG16
Air gap width, mm	1
Permanent magnets (PMs):	
- Type	NdFe40,
- Thickness, mm	3.5
- Relative permeability	1.09967
- Bulk conductivity, S/m	625000
- Residual flux density B_r, Tesla	1.24

A winding diagram is shown in Fig 4.17. Winding is supplied with the rated rms current of 9.2 A.

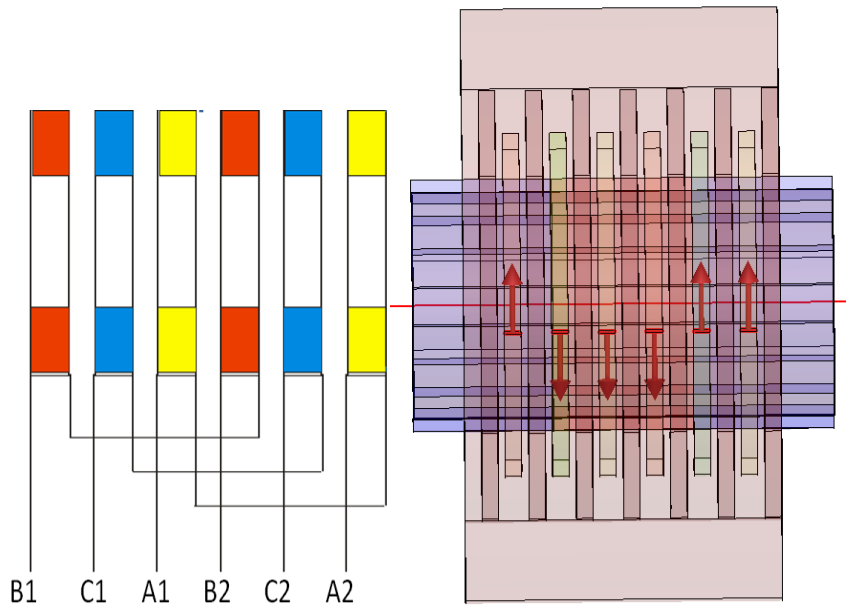

Fig. 4.17 a) Winding diagram of the linear armature, b) Actual current distribution in the winding

4.3.2 Magnetic Flux Density

As it was mentioned in the previous section the magnetic flux density distribution plays a vital role in producing the electromagnetic force. For this reason calculation of magnetic field was carried on in Maxwell 12v 3D.

The calculation was performed for 3-phase currents which at the particular time instant had the values: $i_a = 13A$, $i_b = -6.5A$, $i_c = -6.5A$. At these values the current vector $\imath_s$ is displaced in space by 90˚ of electrical angle with respect to the rotor magnetic flux vector Φ_r (see Fig. 4.9). This gives the maximum electromagnetic force to be produced and it is performed by control circuit (with rotor position feedback in brushless DC motors).

The flux density distribution which was obtained from Maxwell 3D is shown in Fig. 4.18.

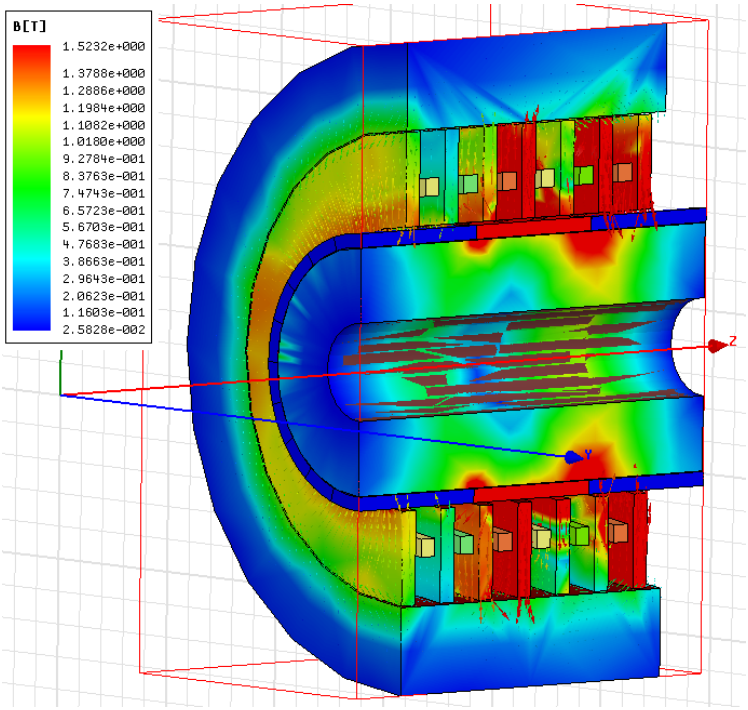

Fig. 4.18 Magnetic flux density in the linear part of TARLPM

The highest flux density is in the stator tooth placed in the middle of the linear armature and is equal to 1.52 T. The asymmetrical distribution of the flux with respect to the center of the

armature is caused by stator currents' reaction. The magnetic density in the stator core does not exceed the permissible value of 1.6 T set for laminated steel.

The magnetic density in the rotor core is 1.1 T. However, as it can be seen from the picture, the density is much higher on magnet borders (S-N). It caused by the intensive magnetic field which is closed between two adjacent magnets of different polarity.

4.3.3 Axial Force

Axial force F_z is calculated at particular time instant when the currents flowing in the winding may be assumed as DC currents with values: $i_a = 13A$, $i_b = -6.5A$, $i_c = -6.5A$. To obtain the maximum value of axial force acting on the rotor, the stator winding was positioned with respect to the rotor as it shown in Fig.4.19.

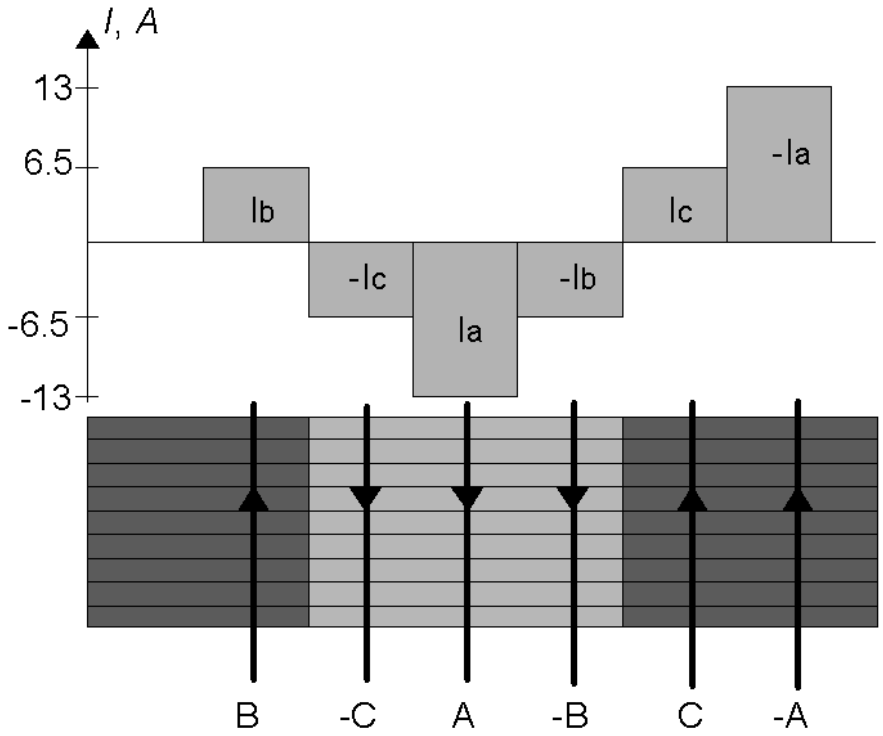

Fig. 4.19 Actual currents to rotor position diagram

Axial force F_z calculated from Maxwell 3D is 653N.

4.3.4 Cogging Force

Permanent magnet linear synchronous motors (PMLSM) exhibit high cogging force which causes a force ripple. The cogging force of the motor is shown in Fig. 4.20

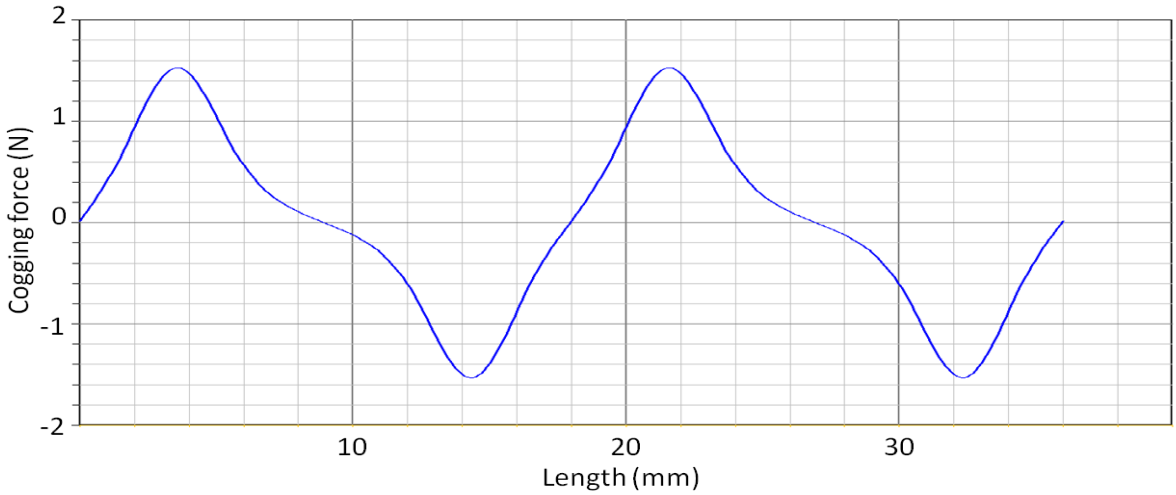

Fig. 4.20 Cogging force of the linear motor when magnets are not skewed

As it was mentioned in previous section, the cogging effect can be minimized significantly if the magnets on the rotor surface are skewed for one tooth pitch. The rotor of the PM motor with linear armature with skewed magnets for one tooth pitch is shown in Fig. 4. 21

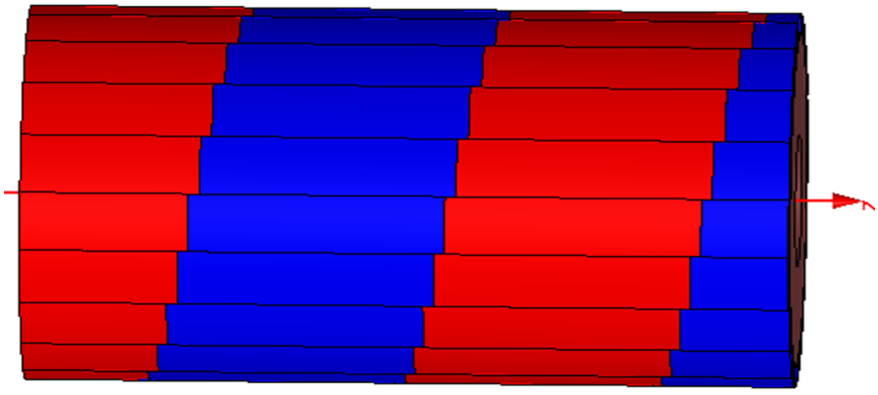

Fig. 4.21 Rotor of the linear motor with magnets skewed for one tooth pitch

The cogging force of the motor with skewed magnets is shown in Fig. 4.22. As it can be seen from obtained results the cogging torque is minimized by 55%.

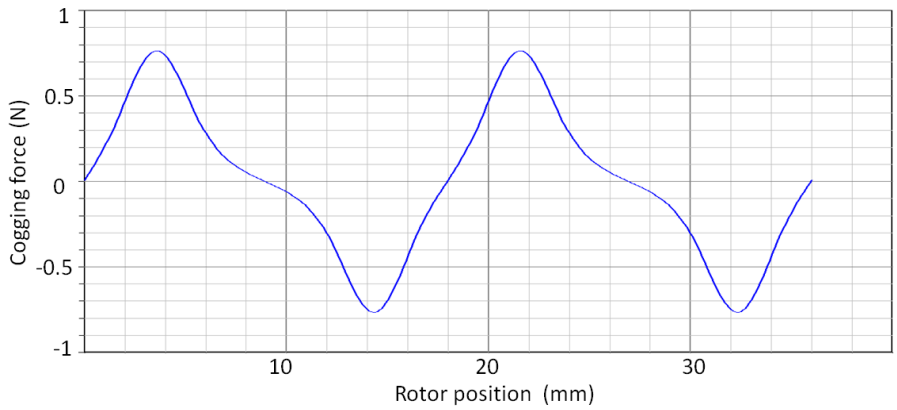

Fig. 4.22 Cogging force of the linear with skewed magnets by one tooth pitch

Despite cogging force is reduced there is still a force ripple. Force ripple minimization is discussed in the section 4.5.

4.4 PM Motor with Two Rotary Armatures

4.4.1 Design Parameters of the Motor

The motor with two rotary armatures is shown schematically in Fig. 4.23.

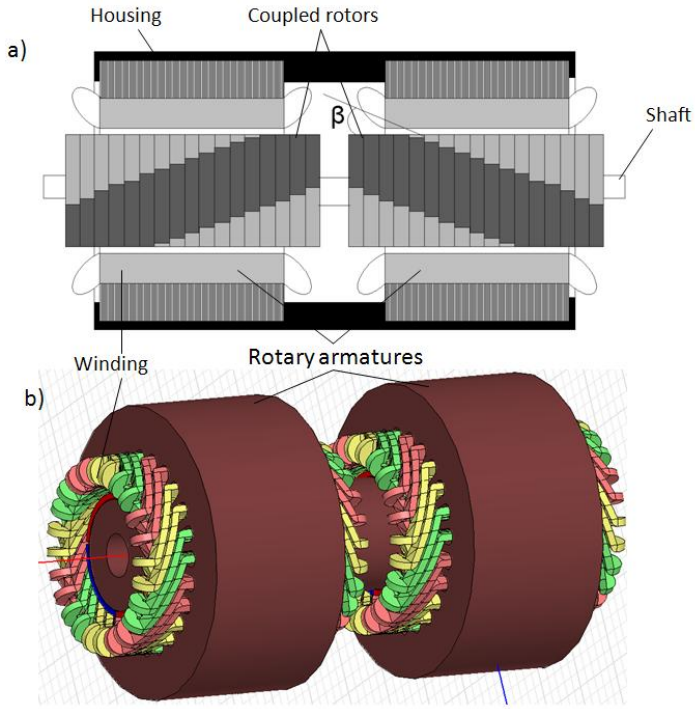

Fig. 4.23 PM motor with two rotary armatures: 2D scheme (a), 3D-view (b)

The stator consists of two rotary armatures. Design parameters of each of the rotary armatures as well as rotors are the same as those discussed in the previous section (see Figs. 4.1-4.5 and Table 4.1). The rotors of the motor are coupled together stiffly. Magnets on both rotors are skewed with respect to a longitudinal axis in opposite direction by an angle β. The rotating magnetic flux generated by each armature interacting with permanent magnets gives raise to the force acting on each part of the rotor in the direction perpendicular to the magnet line as it shown in Fig. 4.24 (for description of the forces acting on the rotor see CHAPTER 1. INTRODUCTION, The motor with two rotary armatures).

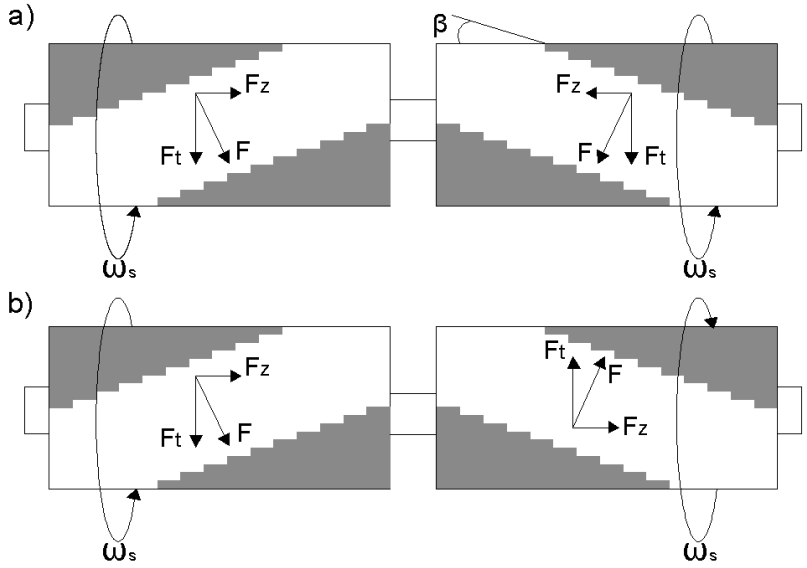

Fig. 4.24 Forces acting on the rotor (ω_s - speed of the armature magnetic field)

4.4.2 Electromagnetic Torque and Linear Force Developed by the Motor

The torque developed by the rotary PM 3-phase motor supplied with sinusoidal currents can be expressed by the equation [11]:

$$T_{em} = \frac{p}{2}\ \lambda_{sd} i_{sq} - \lambda_{sq} i_{sd} \tag{4.7}$$

where p – number of poles; $\lambda_{sd}, \lambda_{sq}$ - flux linkages of d and q axes; i_{sq}, i_{sd} – currents of d and q axes.

In case of non-salient pole machine and a sinusoidal distribution of magnetic field of permanent magnets [11]:

$$T_{em} = \frac{p}{2}\,(\lambda_{fd} i_{sq}) \tag{4.8}$$

where λ_{fd} - the flux linkage of the stator due to flux produced by the rotor magnets.

When the magnets are skewed with respect to stator windings (Fig. 4.25), λ_{fd} is diminishing, thus the torque is reduced too.

By simplifying our reasoning the axial force F_z can be expressed in terms of skew angle β and rotational force F_t as follows:

$$F_z = F_t(\beta)\tan\beta, \quad \text{or} \quad F_z = \frac{T_{em}}{R_r}\tan\beta \tag{4.9}$$

where R_r is the motor radius. Thus the axial flux is a subject of tangent of skew angle and the flux linkage λ_{fd} that is affected be skew angle too.

To determine quantitatively an impact of skew angle β on torque and axial force calculations were carried out using 3D-FEM. The winding was positioned with respect to the magnets as schematically shown in Figs. 4.25 and 4.26

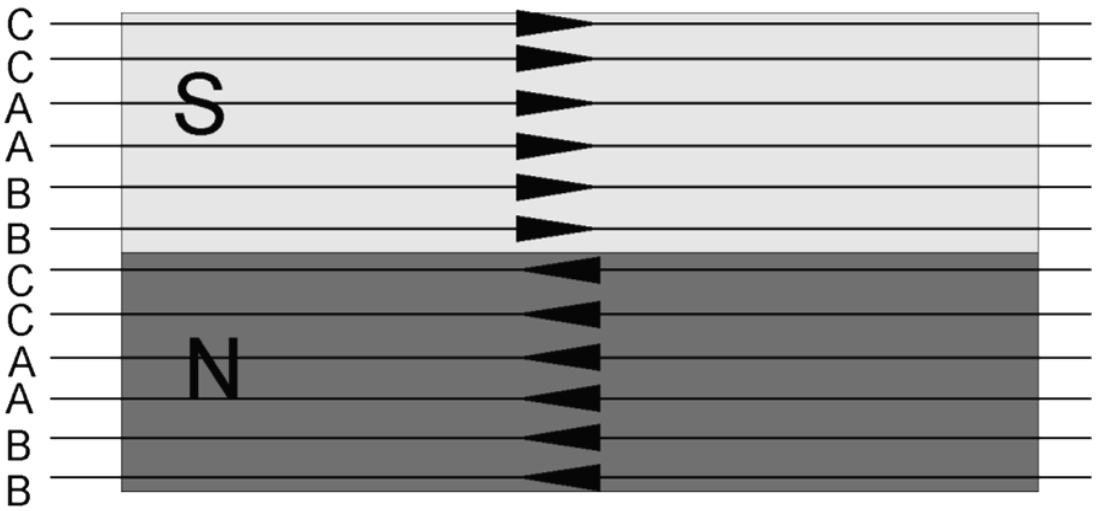

Fig. 4.25 Diagram of actual 3-phase currents positioned with respect to the rotor without skewed magnets

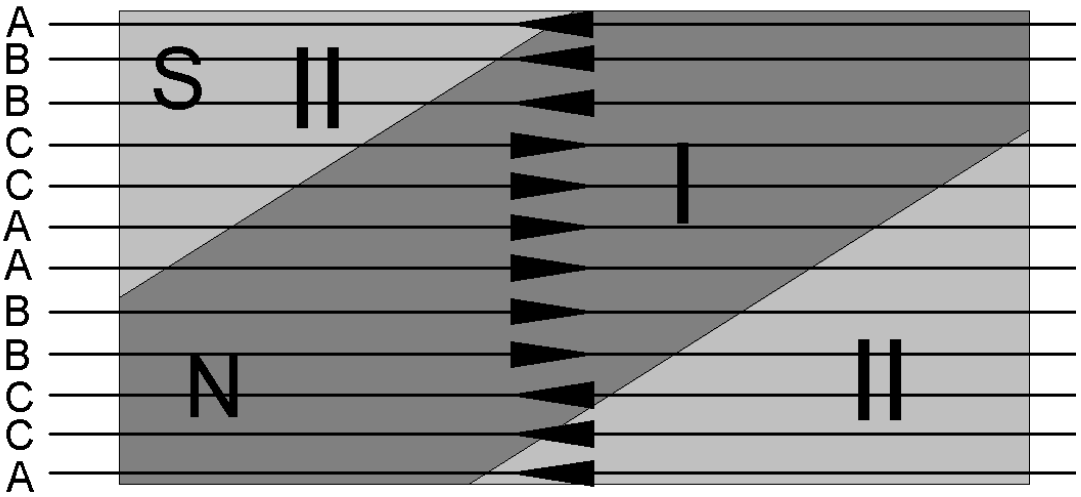

Fig. 4.26 3-phase currents positioned with respect to the rotor with skewed magnets

The calculations were performed for the different values of skew-angle measured in a number of tooth pitches. The values of currents in three phases are the same as in section 4.23. The results of calculations produced by one armature are shown in Figs. 4.27 and 4.28. On the graphs the skew angle β is expressed in terms of skew coefficient k_b calculated as:

$$k_b = \frac{\beta}{\beta_t}$$

where B_t is the angle of one tooth pitch. Consequently, the coefficient k_b is the skew angle measured in number of teeth.

The torque decreases almost linearly with the increase of skew angle. If the flux linkage were not changed with magnet skewing the torque would change according to:

$$T_{em} = T_{em}(\beta = 0)(\cos\beta) \qquad (4.10)$$

as it was marked with a curve line with the increase of skew angle β in Fig. 4.27. Due to a diminishing effect of flux linkage the torque decreases more rapidly.

The axial force first increases with the increase of skew angle, then decreases due to decreasing of the flux linkage.

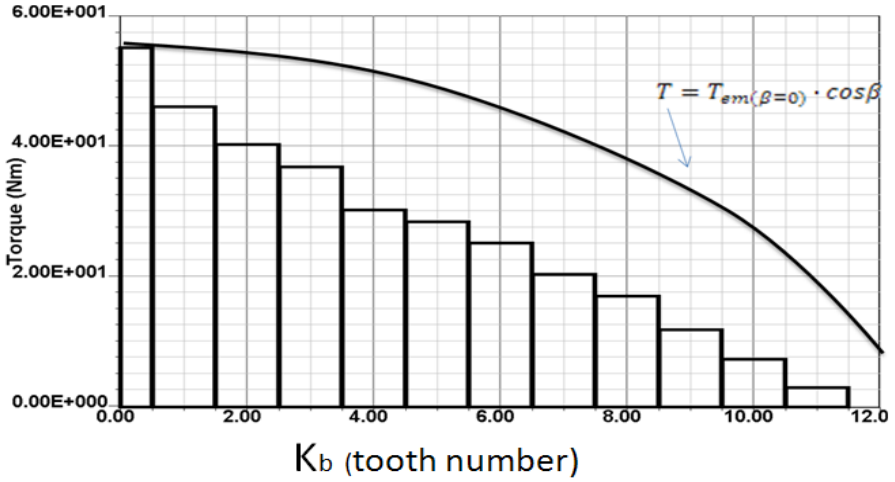

Fig. 4.27 Torque variation

The curve line (Fig. 4.28) shows the axial force changing if there is no influence of the skewing on the flux linkage. This force would change according to:

$$F_z = \frac{T_{em}(\beta=0)}{R_r} \tan \beta \qquad (4.11)$$

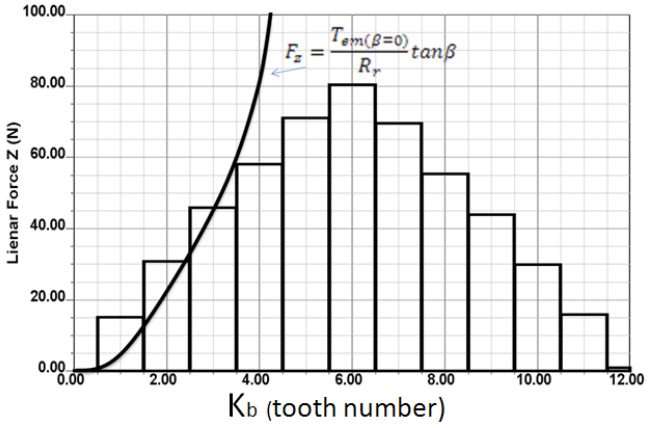

Fig. 4.28 Linear force variation

Referring the analysis of torque and axial force to the motor with two rotary armatures the best operating conditions are if magnets on both parts of the rotor are skewed by one pole-pitch (6 tooth pitches for this particular design). In this case the PM brushless motor with TDMF supplied by the rated current of 9.2 A, develops:

- **53.55Nm torque**, if the both magnetic fields rotate in the same direction;
- **162.3N axial force** if magnetic fields rotate in opposite directions.

By manipulating the supply voltage any desirable direction of the rotor motion can be achieved.

4.4.3 Torque Ripple Reduction

The torque ripple in case of slotted stator is caused mainly by cogging torque component. This component can be minimized by skewing the magnets by angle being the multiplication of one tooth pitch. This was discussed in subsection *4.2.5 Cogging Torque.*

The torque ripple can be further reduced if the magnets on both parts of the rotor are displaced in rotating direction by an angle of one phase winding.

By displacing one rotor by one slot for an angle τ corresponding to one half of the cogging torque period (see Fig.4.29), the torque ripple generated by each air gap would be with different polarity and similar peak value [10].

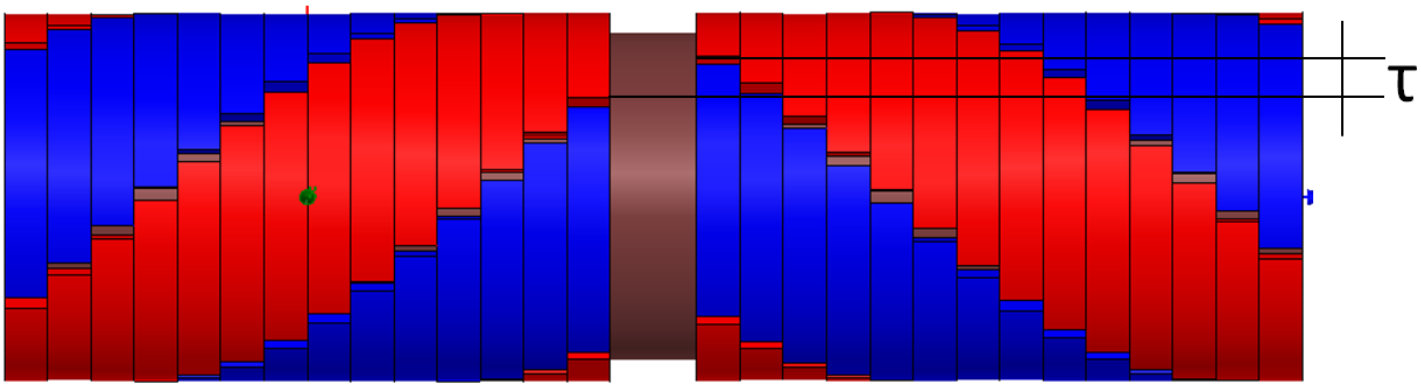

Fig. 4.29 Rotor with displaced magnet poles

To check this idea of torque ripple reduction calculation have been done using 3-D Maxwell 12v software. Torque ripple developed by the motor for displaced and non-displaced rotor magnets is shown in Fig. 4.30.

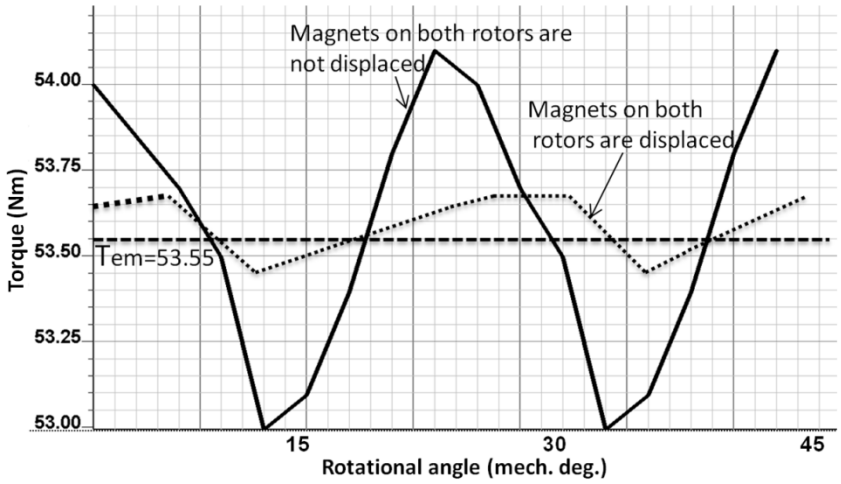

Fig. 4.30 Torque developed by the motor with two rotary armatures (with the rotor shown in Fig. 4.29)

By applying the proposed method, torque ripple of the motor is reduced for 89%. However, the average torque also got reduced from 55.2 to 53.55 Nm due to the displacement of the magnets with respect to the winding as it was shown in Fig. 4.26. The same effect of torque ripple reduction can be achieved by displacing two armatures in rotating direction of the rotor by an angle of one phase winding.

4.5 PM Motor with Two Linear Armatures

4.5.1 Design Parameters of PM Motor with Two Linear Armatures

PM motor with two liner armatures is shown schematically in 2D (a), and 3D (b) view in Fig. 4.31. The stator consists of two linear armatures. Design parameters of each of the linear armatures are the same as those discussed in the subsection 4.3.1. The rotors of the motor are coupled together stiffly. Magnets on both rotors are skewed with respect to a longitudinal axis in opposite direction by an angle β.

The axial magnetic flux generated by each armature interacting with permanent magnets gives raise to the force F acting on each part of the rotor in the direction perpendicular to the

magnet line as it shown in Fig. 4.32 (for description of the forces acting on the rotor see CHAPTER 1. INTRODUCTION, The motor with linear armatures).

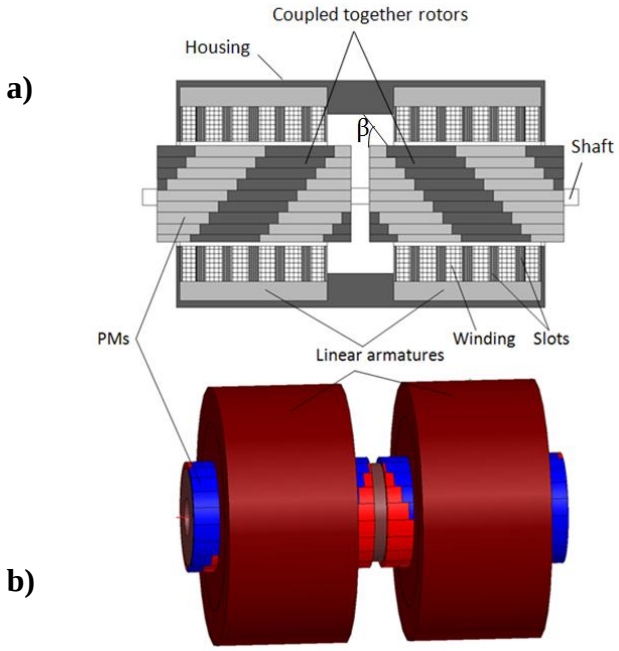

Fig. 4.310 PM motor with two linear armatures

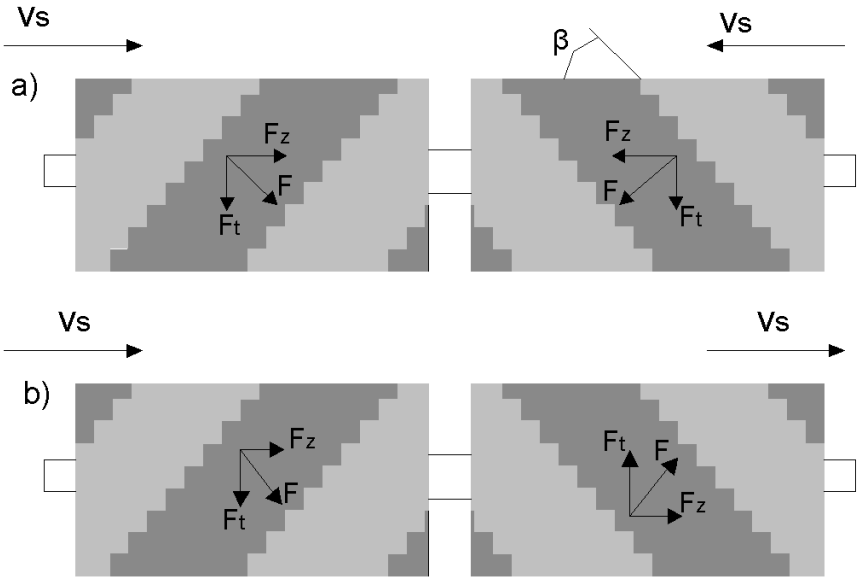

Fig. 4.32 Forces acting on the rotor

4.5.2 Axial Force and Torque

Axial force and torque variations when magnets get skewed for integer number of slot pitch (1,2,3…6) are very similar to those demonstrated in the section 4.3.2 for the TRLMPM with rotary armature. But in this case with increase of skew angle the axial force F_z will decrease, and the rotary force F_t will increase. That is why it was decided not to discuss how magnet skew angle affects rotary and axial forces.

The optimum operating conditions of the motor are obtained when magnets are skewed for one pole-pitch (3 slot-pitches) and winding is positioned when the magnet poles are maximally embraced by the winding pole (Fig. 4.33).

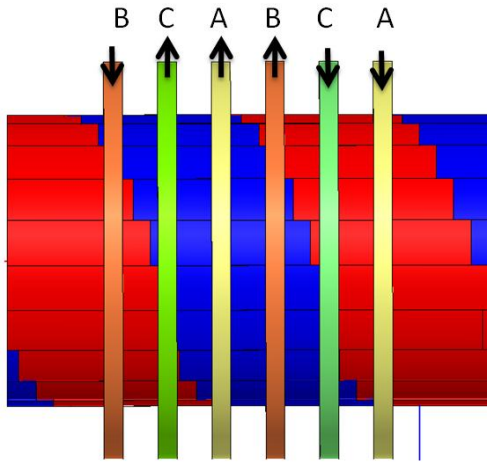

Fig. 4.33 Position of the winding with respect to rotor position

To determine the force produced by two parts of the motor it was modeled in 3-D FEM using Maxwell 12v software package. The calculations were done of the same currents as linear armature of the rotary-linear motor in the section 4.3.

Thus, the motor with two linear armatures develops:

- 11.6 Nm torque, if the both magnetic fields are traveling in the same direction;
- 567.1 N axial force if magnetic fields are moving in opposite directions.

By manipulating the supply voltage any desirable direction of the rotor motion can be achieved.

4.5.3 Force Ripple Reduction

There are many papers written on the subject of force ripple minimization in linear motors [12,13]. However, some of them propose ideas which are difficult to implement in manufacturing process. The techniques presented in this thesis deals with the PM or armature shifting that does not introduce any difficulty in manufacturing. The benefit is achieved both in cogging torque reduction and in emf harmonic reduction.

The proposed technique is based on shifting one armature with the respect to other one for one tooth pitch length τ (Fig. 4.34). As a consequence, the force ripple of the motor was significantly reduced from 50 to 10N. It is 80%. Force ripples to and after armature shifting is shown in Fig.4.35.

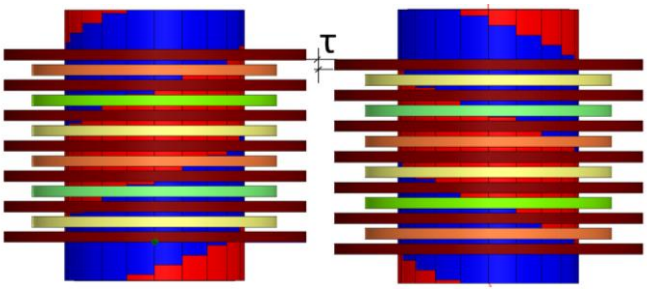

Fig. 4.34 Displaced armatures by one tooth pitch

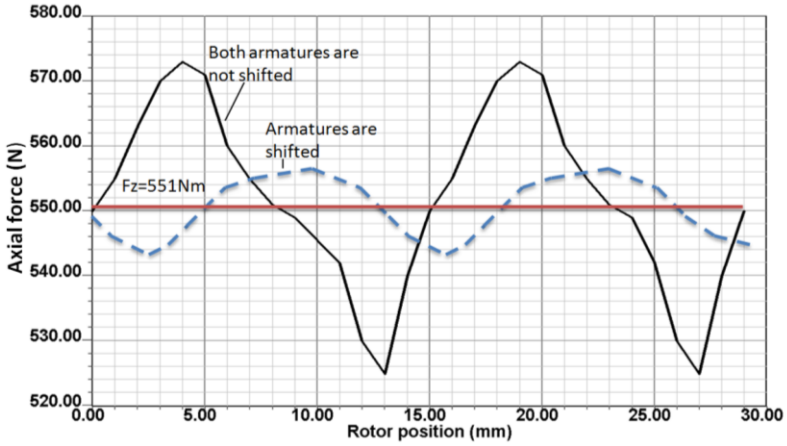

Fig. 4.35 Electromagnetic force calculated for the motor with two linear armatures with the skewed magnets on the rotor by one pole pitch

CHAPTER 5: CONCLUSIONS AND FUTURE SCOPE OF STUDY

5.1 Conclusions

The PM AC motors which are the objects of the thesis allow performing motion in rotary and linear directions. This is achieved by combining two PM motors with rotary and linear, two rotary, or two linear armatures) and by skewing PMs on the rotors in opposite directions.

Three versions of PM AC motors with TDMF were studied:

- motor with rotary and linear armature;
- motor with two rotary armatures;
- motor with two linear armatures.

To determine the magnetic field, torque and force produced by the motors FEM methods were used which allowed to simulate the motor in 2-D and 3-D space. The results of torque and axial force calculations of particular version of the motor are enclosed in Table 6.1.

From the results presented in this thesis report the following conclusions can be made:

- The highest value of torque can be achieved when the motor consists of rotary and linear armatures.
- The highest linear force is produced by the motor with two linear armatures.
- In case of the motor with two rotary armatures and the motor with two linear armatures the torque and linear force can be achieved when the magnets are skewed by one pole-pitch.
- The main component of torque and force ripple is the cogging torque and cogging force.
- The cogging torque and force can be significantly reduced by skewing PMs by one pole pitch with respect to the stator winding.

- To reduce further torque and force ripple the magnets on the adjacent rotor parts should be displaced by one tooth-pitch (motor with 2 rotary armatures), half of tooth-pitch (motor with two linear armatures).
- The main advantage of the proposed motors is that each of them replaces two separate motors and its mechanical parameters (torque, force, speed) can be easily controlled.

Torque and axial force of three motors are in Table 6.1

Table 5.1 Torque and axial force developed by the motors with TDMF

Machine type	Torque (Nm)	Axial force (N)
PM synchronous motor with rotary and linear armatures	55.6	653
PM synchronous motor with two rotary armatures	53.5	162.3
PM synchronous motor with two linear armatures	11.6	567.1

5.2 Future Scope of Study

The objectives that were accomplished in this thesis are related to modeling the motor in 2D and 3D space using FEM in order to determine the electromagnetic torque and force in steady state conditions.

The next stage which has to be done towards successful completion of study on the motors is the motor dynamics and control. Motor dynamics can be studied using Matlab. Power electronics and control applications can be modeled in Simplorer (Ansoft).

5.3 Possible Practical Use

The motor can be used as a drive for a concrete mixer which is shown in Fig. 6.1

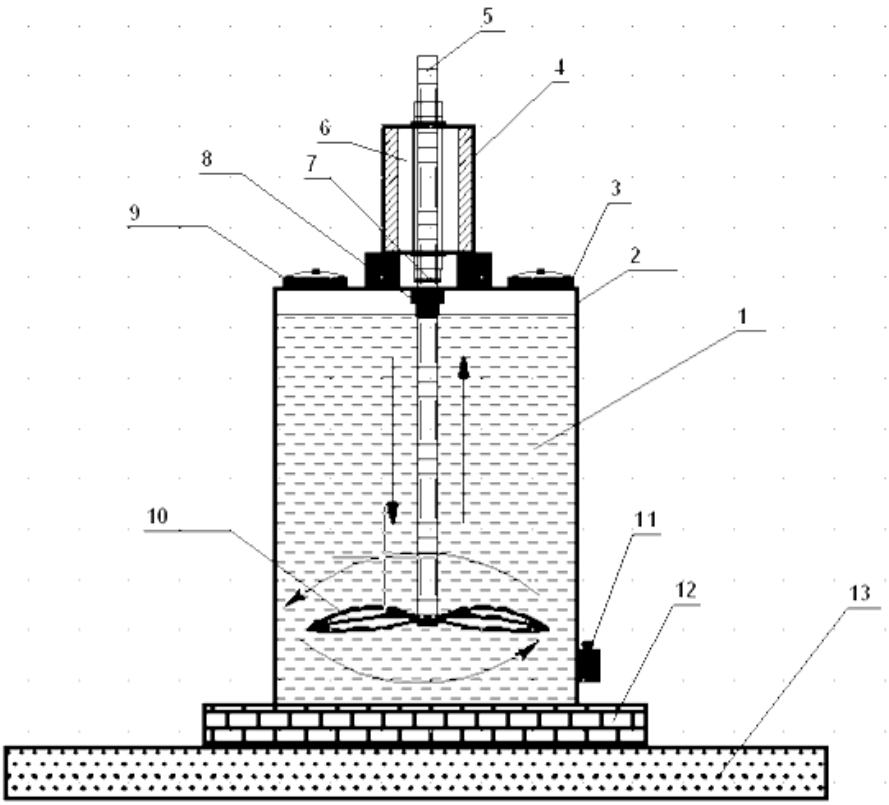

Fig. 5.1 Scheme of concrete mixer: 1- Concrete compound, 2- Fixed bowl, 3- Hatch for loading bulk materials, 4- PM rotary-linear motor, 5- Rotary working part, 6-Motor coil slots, 7- Activator suspension, 8- Brushes-cleaners, 9- Hatch for loading water, 10-Mixer blades, 11- Sliding gate, 12- Steady stand, 13- Base.

Due to high demands of Civil Engineering in producing large amounts of concrete in a short time, and ability to move concrete plants to different locations there is a need for concrete mixers which can be easily set up at the construction yard and can operate quickly and efficiently. A new type of concrete mixer is presented. The mixer consists of a fixed bowl, synchronous PM motor with two degree of mechanical freedom (PMMTDMF), and a mechanical system of a rotary working part connected to blades. The rotor of the motor drives the rotary working part linearly and rotationally. Concrete compound moves helically as a result

of the rotary and linear movement of blades, which provides equal concentration of ingredients at any point of the volume.

Several major cement plants in the USA have been researched by the author. The main disadvantage of today's existing mixers for large volumes of concrete compounds is their complexity in relocation to a construction yard. Because these mixers provide only one degree of mechanical freedom of the rotary working part (rotational), blades are made wide enough in order to embrace the whole volume of concrete during rotation. Therefore, the load torque caused by the compound is very high, which requires a more powerful motor to be selected. As a rule, such mixers are not designed to be set out and set up.

Most of the existing mixers are built with transmission belts which have to be replaced from time to time. Also, such mixers use induction motors as a drive, which consumes more energy. Recent publications by TECO-Westinghouse Motor Company suggest synchronous motors for use in cement plants [14].

BIBLIOGRAPHY

[1] J. Fleszar, E. Mendrela, "Twin-Armature Rotary-Linear Induction Motor", *IEE PROC., vol. 130, Pt. B, #3, May 1983, pp. 186-192.*

[2] E. A. Mendrela, E. Gierczac, "Double-Winding Rotary-Linear Induction Motor", *IEEE Transactions of Energy Conversion, vol. EC-2, #1, 1987, pp. 47-54.*

[3] Jacek F. Gieras, Mitchell Wing, "Permanent Magnet Motor Technology Design".

[4] Maxwell 3D v12, Getting Started Guide, ANSOFT, February 2008.

[5] W.Fei, P.C.K. Luk, "Cogging torque Reduction Techniques for Axial-Flux Surface-Mounted Permanent-Magnet Segmented-Armature-Torus Machines", *IEEE Transactions on Magnetics, 2008, pp. 485-490.*

[6] E. Muljadi and J. Green**, "**Cogging torque Reduction in Permanent Magnet Wind Generators" *January 2002 • NREL/CP-500-30768.*

[7] Z. Q. Zhu and D. Howe, "Analitical Prediction of Cogging Torque in Radial Field Permanent Magnet Brushless Motors", *IEEE Transactions on Magnetics, Vol.28, No.2., 1992, pp.1371-1374.*

[8] Y. D Lao, D.R. Huang, J. C. Wang, S. H. Liou, S. J. Wang, T. F. Ying, D.Y. Chiang, "Simulation Study of the reduction of Cogging Torque in Permanent Magnet Motors', *IEEE Transactions on Magnetics, Vol.33, No.5, September 1997, pp.4095-4097.*

[9] Kartik Sitapati and Rob St. Germain, *Kollmorgen Corp., Radford, http://machinedesign.com/article/reducing-cogging-torque-in-brushless-motors-0601.*

[10] W. Fei, P.C.K. Luk, "Cogging Torque Reduction Technique for Axial-Flux Surface-Mounted Permanent Magnet Segmented-Armature-Torus Machines", *IEEE Transactions on Magnetics, 2008, pp.485-490.*

[11] Ned Mohan, "Advanced Speed Drives", *2007, pp.132-134.*

[12] Nicola Bianchi, Selverio Bolognani, and Alessandro Dalla Francesca Capello, "Back E.M.F Improvement and Force Ripple Reduction in PM Linear Motor Drives", *2004 35th Annual IEEE Power Electronics Conference, Aachen, Germany, 2004, pp.3372-3377.*

[13] Shoji Shimomura, Masayasu Fuijeda and Kastunhiro Hoshino, "Studies to Decrease Cogging Force and Pulsating Thrust in the Prototype Linear Permanent Magnet Vernier Motor", International Conference on Electrical Machines and Systems, 2008, *IEEE Transactions on Magnetics, February 2009,* pp.3417-3422.

[14] Mark Fanslow, "Considerations in the selection and application of AC and DC motors for cement plants", *IEEECement Industry Technical Conference Record,* 2009, pp.1-22.

[15] David Meeker, "Finite Element Method Magnetics – Version 4.0", *User's Manual, January 8, 2006.*

[16] Ernest Mendrela, Janina Fleszar and Ewa Gierczak, "Modeling of Induction Motors with One and Two Degrees of Mechanical Freedom", *Kluwer/Dordrecht/London*, 2003, pp 50-55.

[17] Iwamoto Masatami , Ohno Eiichi , Itoh Toshio, Shinryo Yoshiyuki, "End-Effect of High-Speed Linear Induction Motor", *IEEE Transactions on Industry Applications*, Nov. 1973, pp.632 – 639.

[18] J. F. Eastham, M. J. Balchin, P.C. Coles, "Full-Scale Testing of a High Speed Linear Synchronous Motor and Calculation of End-Effect", *IEEE Transactions on Magnetics*, Nov, 1988, pp. 2892-2894.

[19] J. F. Pan, N. C. Cheung, Guagzhong Cao, "A Rotary-Linear Switched Reluctance Motor", *3rd International Conference on Power Electronics Systems and Applications*, 2009.

[20] Tomoaki Mashino, Shigeki Toyama, "Micro Rotary-Linear Ultrasonic Motor for Endovascular Diagnosis and Surgery", *2008 IEEE International Conference on Robotics and Automation*, Pasadena, CS, USA, May 19-23, 2008, pp. 3600-3605.

[21] L. Chen, W. Hofman, "Design of one Rotary-Linear Permanent Magnet Motor with Two Independently Energized Three Phase Winding", *International Conference on Power Electronics and Drive Systems*, 2007, pp. 1372-1376.

[22] E. Mendrela, "Electric Machines", Course Pack, Louisiana State University, 2004.

[23] G. R. Liu and S. S. Quek, "Finite Element Method", A practical course, Linacre House, Jordan Hill, Oxford OX 8DP, 2003, pp.3-9.

VITA

Oleksandr Dobzhanskyi was born in Kiev (Ukraine) in July, 1985. He completed his schooling at Chernyatyn Secondary School.

He graduated with distinction from Kiev National University of Construction and Architecture with a degree of Master in Industrial Engineering in 2007. He joined the Department of Electrical and Computer Engineering at Louisiana State University in August 2009 to pursue his doctoral degree. He will be awarded the degree of Master of Science in Electrical Engineering in December 2010.